Desalination and Water Treatment
www.deswater.com
doi: 10.5004/dwt.2020.25782

193 (2020) 189–211
July

A new system design of using solar dish-hydro combined with reverse osmosis for sewage water treatment: case study Al-Marj, Libya

A.M. Soliman[a,b], Adil Al-Falahi[c], Mohamed A. Sharaf Eldean[b,*], Monaem Elmnifi[d], Magdi Hassan[e], Basim Younis[f], Abdelnasser Mabrouk[b,g], Hassan E.S. Fath[h]

[a]*Mechanical Engineering Department, Faculty of Engineering, Jouf University, Sakaka, Saudi Arabia, email: amsoliman@ju.edu.sa (A.M. Soliman)*
[b]*Department of Mechanical Engineering, Faculty of Engineering, Suez University, Egypt, Tel. +601139795943; emails: mohammed.eldeen@suezuniv.edu.eg/mwahab31@yahoo.com (M.A. Sharaf Eldean), aaboukhlewa@hbku.edu.qa (A. Mabrouk)*
[c]*Institut Energie systeme und Energietechnik (EST), Technische Universität Darmstadt, Otto-Berndt-Straße 2, Darmstadt, Germany, Tel. + (49) 6151/16 20724; email: adil.al-falahi@est.tu-darmstadt.de (A. Al-Falahi)*
[d]*Department of Mechanical Engineering, Bright Star University of Technology-Briga, Ajdabiyah Libya, email: monm.hamad@yahoo.co.uk (M. Elmnifi)*
[e]*Water technology Department, Higher Institute of Agricultural Techniques, Al-Marj City 25426, Libya, email: magdi.almosmary@gmail.com (M. Hassan)*
[f]*Civil Engineering Department, Higher Institute of Comprehensive Occupations, Al-Marj city 25426, Libya, email: taliba72@yahoo.com (B. Younis)*
[g]*Qatar Environment and Energy Research Institute, Hamad Bin Khalifa University, Qatar Foundation, Doha, Qatar*
[h]*E-JUST Egypt–Japan University of Science and Technology, Alexandria, Egypt, Tel. +201271111740; emails: h_elbanna_f@yahoo.com/hassan.fath@ejust.edu.eg (H.E.S. Fath)*

Received 9 September 2019; Accepted 5 March 2020

ABSTRACT

A novel design of reverse osmosis (RO) membrane is performed for wastewater treatment processes in Al-Marj, Libya. In Al-Marj area, industrial wastewater formed sewage ponds in the region, which posed a great danger to the surrounding environment. Sewage ponds have been formed because of the existence of natural gas and oil refinery stations in that area. The proposed system will recycle the sewage pond wastewater in order to provide approximately 3,500–10,500 m^3/d of freshwater. The produced freshwater is expected to serve around 55,000 inhabitants in a semi-arid area. Reverse osmosis membrane processes will be used for freshwater production. Concentrated Solar Gas Engine will be used as a main source of power for reverse osmosis operation. Solar Stirling dish engine with CO_2 working gas is considered a new vital option in such an application. Hydraulic power system (lower tank, pump, upper tank, and hydraulic turbine) is used as an energy recovery storage system instead of using batteries or diesel generators. The results reveal that the total water price was in the range of 0.65 \$/m^3, and the specific power consumption was not exceeding over 4 kWh/m^3.

Keywords: Wastewater; Reverse osmosis membrane; Trace pollutants; Renewable energy; Solar Stirling engine

1. Introduction

Wastewater disposal is becoming a problem in developing countries as large quantities of municipal waste and industrial effluent are being produced due to increased urbanization and industrialization, respectively. The major challenge is how to deal with the wastewater which is being released at a rate faster than its proper disposal. Moreover,

* Corresponding author.

on the long-term, the use of wastewater in agricultural land will increase the concentration of heavy metals in the soil. These heavy metals include zinc (Zn), cadmium (Cd), copper (Cu), nickel (Ni), lead (Pb), manganese (Mn), iron (Fe), mercury (Hg), and chromium (Cr) [1]. According to the World Bank, "the greatest challenge in the water and sanitation sector over few decades will be the implementation of the low cost of sewage treatment that will at the same time permit selective reuse of treated effluents for agricultural and industrial purpose" [2]. Innovative removal processes include adsorption, new adsorbents, membrane filtration, electro-dialysis, reverse osmosis, and photo-catalysis have been adopted recently.

The problem with the current treatment technologies is the lack of sustainability. The conventional centralized system flushes pathogenic bacteria out of the residential area, using large amounts of water and often combines the domestic wastewater with rainwater, causing the flow of large volumes of pathogenic wastewater. Add to that, salts concentration in wastewater could be massive in the case of costal area, or desert zones. Membranes technology (reverse osmosis (RO)) is considered a unique technique to be used for wastewater treatment. Although desalination is the main application for reverse osmosis, the treatment of wastewater represents an important open market to the RO. The principal industries where reverse osmosis wastewater treatment can be applied, are the pulp and paper industry, the metal processing industry, the textile industry (dye water), and the food processing industry; furthermore, reverse osmosis can be used in the treatment of municipal wastewater [3]. Barbosa Brião et al. [4] shows the effect of use Nanofiltration (NF) and reverse osmosis (RO) processes on rinse water treatment. Uojima [5] showed the ability of using RO membranes for wastewater treatment within a range of 60%–90% of recovery ratio. Numerous large-scale commercial membrane plants are now being used to reclaim municipal wastewater. These plants include 50,000 m^3/d at various West Basin, California, plants, the Kranji 40,000 and 32,000 m^3/d Bedok plant in Singapore. Some of these plants have more than 10 years of experience with membrane technology.

Additionally, even larger plants have recently begun operation (380,000 m^3/d plant for Sulabaiya, Kuwait) or will soon begin operation (270,000 m^3/d plant in Orange County, California, USA, and the 170,000 m^3/d Ulu Pandan plant in Singapore). The magnitude of these RO-based reclamation plants demonstrates the acceptance that this technology has gained recently [6]. Although using of RO membranes is considered beneficial to the wastewater treatment, but it has some limitations concluded in the power support. RO needs sufficient electric power for the sustainability of the high-pressure pump.

One of the major challenges facing the power issue is to power on the RO by the use of renewable energy resources. Solar energy can be used for those purposes, especially in MENA region. The connection between solar energy and RO can be categorized as direct and indirect connections. For indirect connection, Sharaf et al. [7–10] showed the possibilities of using solar thermal power combined with an organic Rankine cycle as a main source of power for reverse osmosis. The results showed that solar organic Rankine cycle gave superior results with respect to specific power consumption while comparing against other solar thermal desalination processes such as multi-stage flash and/or multi-effect distillation [10]. Delgado-Torres et al. [11–13] showed the preliminary design and performance of the use solar organic Rankine cycle for 100–250 m^3/d desalination by the use of reverse osmosis. For direct connections, there are many research activities that been performed about using solar photovoltaic and wind power combined with RO.

However, most of that technology addresses the lower capacities of the solar-PV-RO systems. Some of them used wind turbines, diesel generators, and fuel cells as energy recovery in order to overcome solar uncertainties. Its main feature is that it requires no thermal energy but, rather, mechanical energy in the form of a high-pressure pump. One of the most important reasons for using RO instead of thermal distillation processes is the reliability and the ease of combining with renewable energy resources. Solar and/or wind energies are rightfully deserved to be used with the RO desalination process. Most of the solar applications combined with RO are established based on photovoltaic (PV) technology. Mohamed et al. [14] investigated technically and economically a photovoltaic system powered brackish water reverse osmosis desalination systems. The system was designed to produce and amount of 0.35 m^3/d with specific power consumption around 4.6 kWh/m^3. The main reason for the high water production cost (15–20 €/m^3) was the need of solar batteries to achieve a constant pressure and flow rate for the membranes [14]. Helal et al. [15] studied the economic feasibility of driving RO by PV within low specific power consumption. Three alternative configurations of an autonomous PV-RO unit for remote areas in the UAE were investigated. Helal et al. [15] studied the possibility of using diesel generator for day off periods. The PV-RO was designed for not more than 20 m^3/d (10 h). Helal's work doesn't investigate the effect of diesel emissions on the environment. Manolakos et al. [16] presented a technical characteristic as well as an economic comparison of PV-RO desalination systems. The PV system consisted of 18 Arco-Solar mono-crystalline PV panels, with total peak power of 846 W. Manolakos et al. [16] system has a capacity of 0.1 m^3/h and the specific energy recovery of that system has been experimentally found to be in the range of 3.8–6 kWh/m^3. The cost of 7.77 €/m^3 is estimated by Manolakos et al. [16] work. The Manolakos work does not investigate the large-scale production based on PV power. Ahmad and Schmid [17] studied the design of a PV powered small-scale reverse osmosis water desalination system. It was found that the cost of producing 1 m^3/d of freshwater using the small PV powered RO water desalination systems is 3.73 $ [17]. Tzen et al. [18] studied the design of an autonomous PV-RO system able to cover potable and other water needs of a rural community in Morocco. That study was built based on 0.5 m^3/h powered by 7.5 kW of high-pressure pump power (SPC = 15 kWh/m^3) [18]. For relatively medium/large capacities Ahmed et al. [19], Ghenai et al. [20], and Murat [21] studied the variable load on the RO based on variable productivity. The system was designed based on PV/HWT/RO configuration [19–21]. Laissaoui et al. [22] evaluated the operation of large-scale reverse osmosis units in combination with different solar power plants, both, concentrating solar power (CSP) and photovoltaic (PV) under variable load conditions. Also, Wang et al. [23] presented a

100% renewable energy system for RO desalination plant. Wind power was presented in Wang proposal [23].

It is clear from the literature that the combination between RO and PV is considered a promising solution for the energy crises related to solar desalination technologies. However, most of it are more suitable for low capacities in case of price comparing. Add to that, the cost/life of batteries is massive and would increase the total water price. The example of Laissaoui et al. [22] showed that it is anticipated to generate a range of 8–13 MWe for RO high-pressure pump by the PV which is considered massive load on PV plant. At the same time, some other literatures proposed a system that can utilize hydropower as a storage system for sun-off periods instead of using batteries in PV systems [24–29]. Most of such hybrid systems were focused on PV/wind as a primary recovery beside small hydropower as battery storage. Add to this, the location of hydropower station should be in relatively high altitude above the RO location. This work has not been investigated before. In this work, a novel study is introduced regarding solar hydropower for wastewater reverse osmosis purification processes. The current study completely differs from the previous studies from the side of using the solar energy combined with hydropower technology. In this work, a concentrated solar gas engine (CSGE/Stirling) is used as the main source of power instead of using PV or PV/HWT. Hydropower plant will be acting as a huge hydro-battery system. Concentrated solar Stirling engine (CSSE) is considered a powerful technique as a power source for RO high-pressure pump. The combination between CSSE and RO was not investigated before especially for large capacities operation. It has some features such as:

- The high fluid temperature attainable by the two axis tracking solar parabolic dish leads to the high conversion efficiency of solar power to electricity (for a heat engine). Conversion efficiency approaching 36% has been achieved (vs. 17%–20% for PV). The solar parabolic dish Stirling engine system can be used as a relatively small-distributed power source, because a single unit is self-contained. By combining many of the units, MWe levels of electricity from solar power can be produced.
- The solar parabolic dish Stirling engine has only a minimal water requirement. The engine is air cooled, so no cooling water is needed and the performance penalty associated with dry air condenser cooling for a steam power plant does not enter into the picture.

In this novel study, Al Marj city, Libya (Longitude: 20.833°, Latitude: 32.5°) is pinpointed as the location of study in this work. Analysis of the soil in the location of operation is presented in order to give an indication about the solids and heavy metals concentrations in the wastewater and underground water. Meteorological data of the location of operation is also presented. Design and optimization of different capacities of the wastewater treatment system by RO process will be investigated and evaluated. Mathematical model for the proposed system is performed. The proposed system model is developed by the authors by the use of REDS software Library environment [30,31]. Techno-economic optimization issue is highlighted in this work in order to reduce the specific power consumption, kWh/m^3, power, kW, system costs, $, and total water price, $/m^3.

2. Al-Marj City, Libya case study

2.1. Wastewater problem and analysis

Al-Marj city, Libya (Longitude: 20.833°, Latitude: 32.5°) is located on the northeastern coast of Libya and the administrative seat of the Marj District. It lies in an upland valley separated from the Mediterranean Sea by a range of hills and part of the Jebel Akhdar Mountains. Al Marj lagoon is located in the east of the city to collect sewage and wastewater. Its position as an agricultural area places a strong emphasis on maintaining the quality of the local environment and means that the smart management of wastewater is very important in the region. The main challenge in the location is the existence of dramatic mountain terrain which considered not an ideal landscape for the housing of sewage treatment plants. The rugged nature, mountainous landscape, and hillside location mean that the main wastewater treatment plant is only a few hundred meters from the city center.

The pumping station management system supervises a pumping station that pumps 5,249 m^3 of liquid waste per day to the treatment plant. The Sanitation Company, the organization responsible for managing the sewage system in the area, must ensure that treated wastewater is discharged directly to the pond complies with strict environmental standards. The following diagrams show the overall scheme of the system and the general plant that refers to the location of the different parts. Fig. 1 shows a photograph of the location of the wastewater treatment plant in Al-Marj city, Libya. Another wastewater treatment plant is located in the city of Al-Marj Libya, 2,000 m east of the city, which is unemployed.

This plant works by sedimentation system, where the proposed project is aiming to add the membrane system for wastewater treatment. The wastewater stream from the city is used to be pumped and accumulated in the outside city sewage pond. The total pond area is nearly about 150 ha, which is 1,065,625 m^3 of disposal wastewater (Fig. 2). The laboratory analysis of 16 samples have been conducted near the drainage pond at different depths and distances [47]. The collection of soil samples were made during the summer based on four farms surround the main sewage pond and at different distances from the edge of the sewage pond (2, 10, 18, and 26 m). Soil strength, pH, EC, organic matter, and organic carbon were analyzed. The results show that the soil of the study area was mostly muddy, full filled with mud and clay which is generally alkaline soil where pH values were ranged from 7.17 to 8.42 [47].

The values of electrophoresis ranged from 4.84 to 7.5 Ms/cm, while the organic matter values for the soil were ranged from 2.7% to 3.4% [47]. The organic carbon values in the soil were ranged between 1.6% and 1.9% [47]. The concentration of available phosphorus was between 42.74 and 54.41 ppm while the total nitrogen values in the soil were between 0.06% and 0.24% [47]. The analysis also discovered that the levels of heavy metals in all sites were lower than the normal limits, where the average concentration of Zn, Fe, Cu, Pb, Cd, Co, are 0.9, 0.91, 0.54, 0.6, 0.05, 0.55 respectively. The percentage of total dissolved salts TDS was ranged between 1,386 and 1,490 ppm. Tables 1–3 show some soil data analysis that be examined at the location of operation.

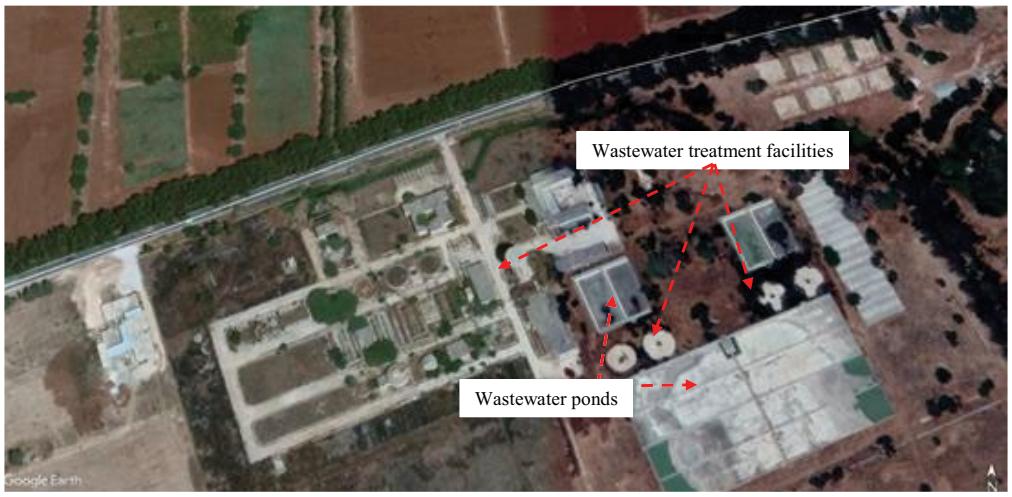

Fig. 1. Photograph shows the wastewater treatment plant in Al-Marj city, Libya.

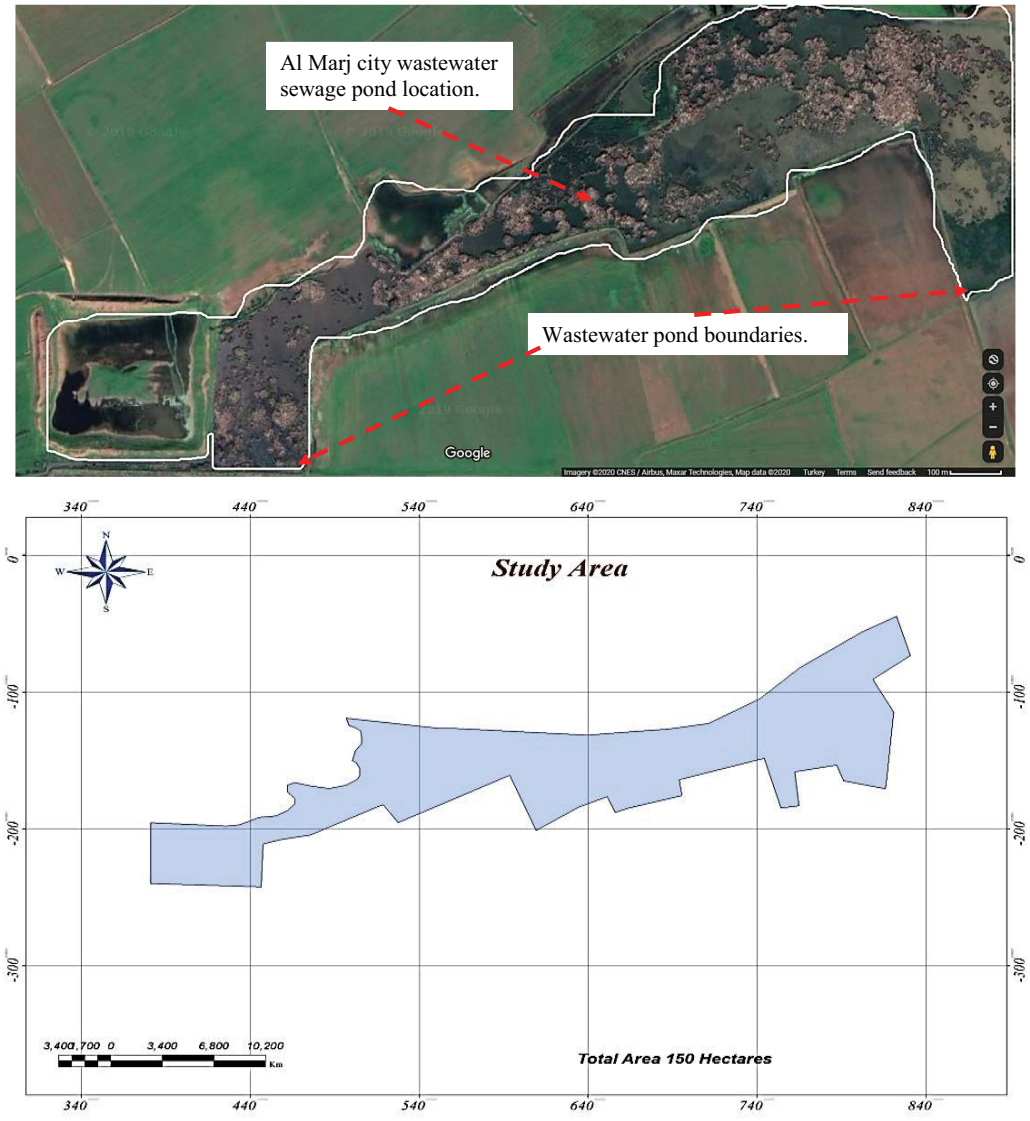

Fig. 2. Plan view of the sewage pond area located in Al-Marj, Libya.

Table 1
Soil data sample from Al-Marj, Libya [47]

E.C, Ms/cm	O.M%	O.C%	N%	P, ppm	pH	Distance from pollution, m
7.500	3.35	1.95	0.062	46.72	7.75	2
6.470	2.95	1.72	0.112	54.32	7.76	10
4.860	2.75	1.60	0.219	42.52	7.76	18
4.810	3.42	1.98	0.118	42.70	7.77	26

E.C, Electrical conductivity; O.M, Organic matter; O.C, Organic carbon; N, nitrogen; P, Phosphor; pH, Hydrogen acidity; Ms/cm, milli Siemens/centimetre; ppm, part per million.

Table 2
Chemical properties of some soil samples from Al-Marj, Libya [47]

T.D.S Meq/100 g	SO_4^{2-}	HCO_3^-	CL^-	K^+	Na^+	Mg^{2+}	Ca^{2+}	Depth	Distance from pollution, m
20.83	14.91	2.47	27	1.5	14.30	5.22	11	0–10	
21.07	13.88	2.41	23	1.42	13.21	7.51	14	15–25	2
21.15	15.89	1.8	20	1.27	14.11	8.13	15	25–40	
19.98	1	0.8	12.10	0.03	15.65	3.50	2.2	0–10	
23.94	3.7	2.10	13.25	1.29	13.91	4.25	5.4	15–25	10
23.87	1.2	1.35	13.70	1.11	13.69	4	9.7	25–40	
21.05	4.93	1.55	17	0.76	10	4	7.51	0–10	
18.84	4.53	1.5	15	1.48	11	4	7.52	15–25	18
20.63	3.66	1.3	16	0.69	10	3	9.42	25–40	

Ca^{2+}, calcium ion; mg^{2+}, magnesium ion; Na^+, sodium ion; K^+, potassium ion; Cl^-, Chloride ion; HCO_3^-, Bicarbonate ion; SO_4^{-2}, Sulfate ion; CO_3^{-2}, Carbonate ion; T.D.S, total dissolved salts; Meq/100 g, milli equivalents/100 9.

Table 3
Concentration of heavy metals in wastewater, ppm based on a soil sample from Al-Marj, Libya [47]

Co	Cd	Pb	Cu	Fe	Zn	Distance from pollution, m
0.5517	0.109	0.1287	0.0112	0.0874	0.0874	2
0.5503	0.0142	0.2023	0.102	1.698	0.1518	10
0.5509	0.1176	1.9128	2.076	0.768	3.3072	18
0.5528	0.0114	0.1961	0.0544	1.1222	0.0832	26

Co, cobalt; Cd, Cadmium; Pb, Lead; Cu, Copper; Fe, iron; Zn, Zinc.

Table 1 represents the soil data according to the electrical conductivity, organic material, organic carbons, nitrogen, phosphor, and pH. The electrical conductivity was about 4.8 Ms/cm at 26 m and the organic material percentages were 3.35% up to 3.42% at 26 m distance. The nitrogen and organic carbon percentages were 0.118% and 1.98% respectively. Table 2 represents the chemical compositions that been analyzed in the soil samples. At a distance of 10 m, the Ca^{2+} was ranging between 2.2 and 9.7 according to the sewage pond depth. The chloride ion was ranging between 12 and 13.7 at 10 m and 15–17 at 18 m distance. Table 3 represents the concentration of heavy metals in wastewater in ppm according to the addressed distances. Fe was found relatively high within the range of 0.087–1.698 ppm. Zn, Cu, and Pe compounds are recorded too high at 18 m with values of 3.307 ppm, 2.076 ppm, and 1.912 ppm, respectively. It is clear from the analyzed tables that the percentages of salts deposited in the soil were concentrated in large amounts and at different distances. This also harms the soil conditions and increases the percentage of salts deposited in the groundwater.

Although the wastewater sewage pond causes some problems, but it might be used as the main source of freshwater supply to Al-Marj city in case of use RO technology. Table 4 shows the data analysis of the station which includes the needed values of freshwater per day for Al-Marj city, Libya.

Based on the available data, the analysis of the required freshwater is shown as follows:

- Design flow, M_d can be calculated based on the city population, discharge of the capital, and the ratio of water reaching the station (=~0.8). The population of the city is about 55,000 citizens and the design is based on the future population of approximately 110,000 citizens.

Table 4
Data analysis for Al-Marj, Libya wastewater treatment

Indicator	Value
Per capita discharge rate	115 L/d
Design population	55,000 citizens
Organic load per person	50 g/d

$$M_d = 55{,}000 \times 115 \times 0.8 = \frac{5{,}249{,}750L}{\mathrm{d}} = \frac{5{,}249\mathrm{m}^3}{\mathrm{d}} \quad (1)$$

- Additional water consumption resulting from the extra resident's activities, and the sewage network of rainfall are estimated as 85 m^3/d. Therefore; the design flow would become:

$$M_d = 5{,}249 \times 85 = \frac{5{,}334m^3}{\mathrm{d}} = \frac{222\mathrm{m}^3}{h} \quad (2)$$

- Sludge flow calculation based on the daily production of organic materials by reference [47] is about 50 g per citizen. Organic materials is then calculated as:

$$\mathrm{OM} = 55{,}000 \times 0.05 = 2{,}750\ \mathrm{kg} = 2.75\ \mathrm{ton} \quad (3)$$

It is clear from the water demand calculations that reverse osmosis can serve and produce the essential freshwater in the range of 3,500–10,000 m^3/d. It may also help by reducing the salinity of the underground water regardless the power source needed for RO plant. For the use of renewable desalination technique, meteorological data is provided in the next part.

2.2. Solar data analysis

This part is to highlight the solar potential data analysis of Al-Marj city, Libya. The main reason for this is to discover the potential power of renewable energy available at the location of operation. The available data were obtained by Global Solar Atlas [32]. Table 5 shows the important and vital information about solar potential at the location of operation. Table 5 shows that the global horizontal irradiation (GHI) is around 5.359 kWh/m^2, the direct normal irradiance (DNI) is about 5.307 kWh/m^2 and the diffuse irradiance in the range of 1.89–1.940 kWh/m^2. Thence, the study location has a great potential of solar energy allowing sufficient use of solar thermal power as a main prime mover for reverse osmosis plant. The sunshine hours almost 11 h with total solar power equal to 19,560–20,000 kWh/m^2/y. Fig. 3 shows the solar radiation results based on solar radiation model calculations [33,34]. The figures show that the daily average radiation is ranges between 10 and 40 MJ/m^2 (Fig. 3b) with monthly average from 2 to 7 MJ/m^2 (Fig. 3d). The DNI along one year is in the range of 400–900 W/m^2 (Fig. 3c). Figs. 3e and f show the variation of solar zenith and incidence angles, respectively. It is clear that solar energy should be used for reverse osmosis desalination plant regarding to its potential at the location of operation.

3. Proposed system, methodology, and assumptions

The combination between renewable energy and RO process has been considered under attention during the last decade. Easy of coupling, reliability, sustainability all of these issues have been considered the backbone reason of the raise of this technology. The easiest and cheapest method is to use direct electrical power generation from the sun to operate RO directly. Concentrated solar gas engines is highly recommended for such purpose especially while dealing with high rate of power. The power conversion of CSGE is relatively high while comparing against the PV conversion. Therefore, the proposed system contains RO plant, CSGE field, and hydropower system (upper tank, lower tank, hydro turbine, and pump) for power recovery instead of batteries. The proposed model configuration under matlab/Simulink environment has been shown in Fig. 4. The proposed system is modeled by the use of REDS software [31]. SDS is a developed software library as a part of REDS program library developed by Sharaf et al. [30,31]. The model is operated under design mode of modeling technique, which calculates unknown parameters such as areas, dimensions, mass flow rates, energy streams, exergy, cost streams, and the entire process temperatures or any other calculated physical properties. For desalination processes, it becomes very important to specify the freshwater capacity, hence, the electricity load will be calculated. In this work, the desired product capacity (specified in m^3/d) is assigned as a known parameter in order to calculate the electricity load on the RO pump. The electricity load will be responsible for the calculation of CSGE and/or the hydropower design specifications. The design limits and the calculated parameters of the proposed units are illustrated in Table 6. Based on a previous work by the authors [34], CSSE with CO_2 working fluid is used for this study. The mathematical model of the proposed system is shown in the Appendix.

3.1. RO optimization

It is quite important to minimize power consumption because it has a direct effect on the cost and area. Therefore, best-operating conditions, assumptions, and considerations should be assigned in order to optimize power consumption. In this section, the technical solution to minimize the objective function (total water price, TWP, \$/m^3) is implemented for the RO part. Optimizing the RO part would effect on total power loads. To minimize the TWP, \$/m^3, it is very important to decrease the power load by the RO pump preserving the same freshwater production rate. One of these technical methods is done by the increase of the number of stages. Increasing the number of stages would permit to desalinate the brine waste many times synchronized with dividing the load by each stage and the pressure on the RO pump. For the same case study example (3,500 m^3/d), we've increased the number of stages up to nine stages (9 stages). Table 7 shows that the increased number of stages would decrease the power from values 1,131 kW down to 917.47 kW, that is, the power is decreased by 18%–20%. Thence, the calculated SPC, kWh/m^3 would become 6.3 vs. 7.7 kWh/m^3 for the basic case (no energy recovery devices). The other method is the fixation

Table 5
Solar potential at Al-Marj, Libya [32]

SITE INFO

Site name:	Al Marj, Libya
Latitude:	32.500000°
Longitude:	20.833330°
Altitude:	333 m a.s.l.

SOLAR RESOURCE AND AIR TEMPERATURE

Long-term yearly and daily averages

Global horizontal irradiation [kWh/sq m]:	1956 per year (5.359 per day)
Direct normal irradiation [kWh/sq m]:	1937 per year (5.307 per day)
Diffuse horizontal irradiation [kWh/sq m]:	708 per year (1.940 per day)
Global tilted irradiation [kWh/sq m]:	2142 per year (5.868 per day), for surface tilted at 26° facing 180°
Air temperature [°C]:	18.5

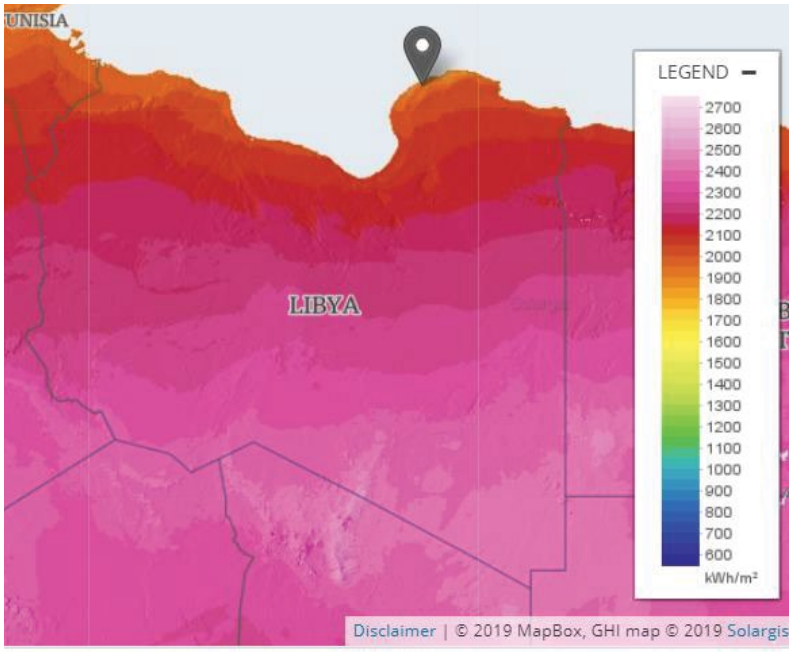

ESMAP Energy Sector Management Assistance Program SOLARGIS

of energy recovery units such as the Pelton Wheel Turbine (PWT) or Pressure Exchanger (PEX) unit (Figs. 5b and c vs. Fig. 5a). Based on a previous study [7,39], PEX device (Fig. 5c) is essential for the operation in RO plants. It can reduce the power consumption by 60%–70% [7] with an operational efficiency reached 98%. Therefore, PEX operation will be considered in this study. RO mathematical model is shown in Appendix-A part.

3.2. CSSE optimization

For CSSE, the operating and design conditions have been considered based on an optimized previous work by the authors [34–37]. Stirling engine has been selected rather than Brayton engine. CO_2 working gas is also considered. Total engine power is 30 kW emerged from four cylinders. Engine piston is 5.5 cm in bore, top cycle temperature is 900°C and

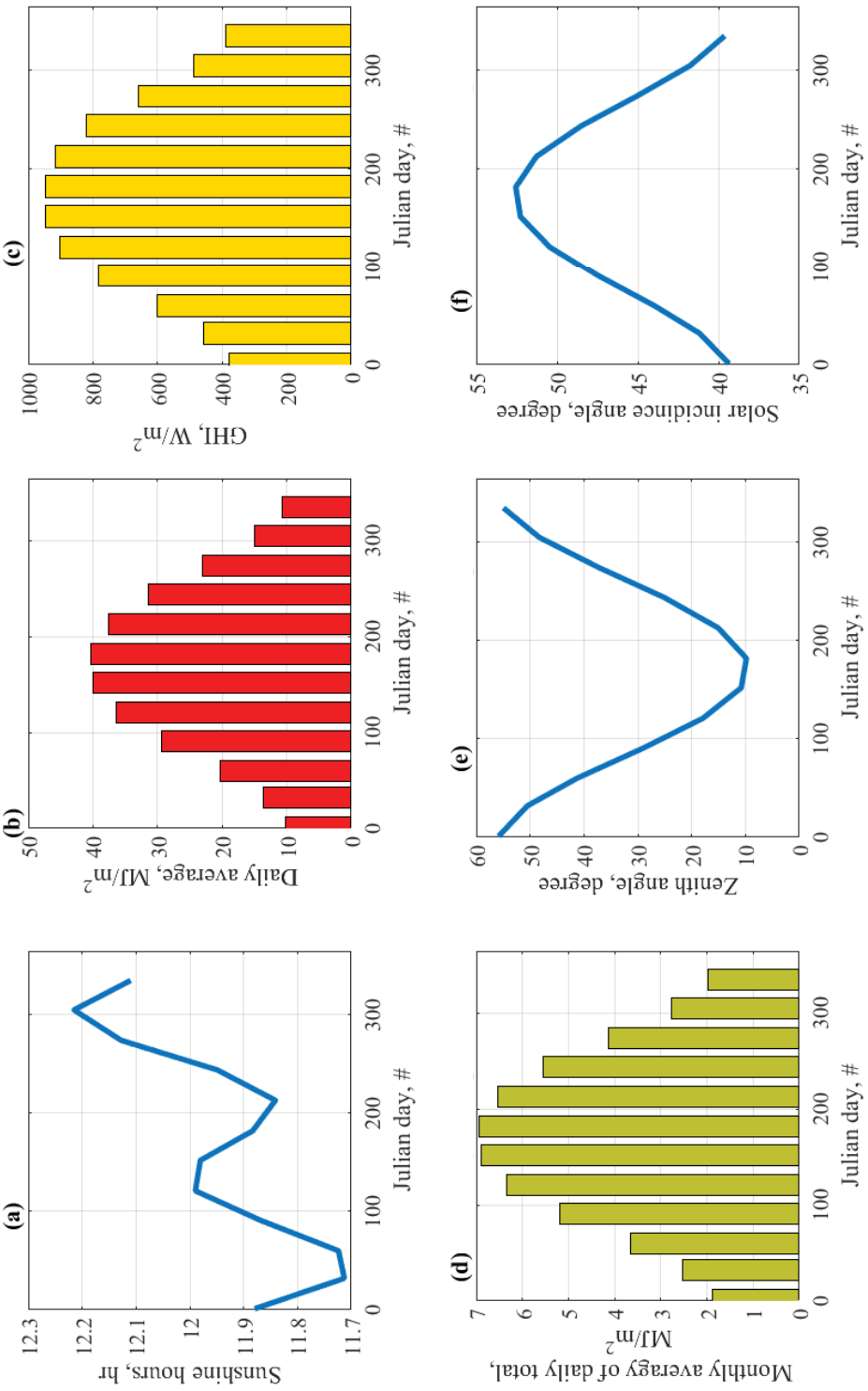

Fig. 3. Solar radiation data results based on the solar radiation model [33,34]. (a) Sunshine hours, (b) daily average radiation, MJ/m^2, (c) GHI, W/m^2, (d) monthly average, MJ/m^2, (e) solar Zenith angle, and (f) solar incedince angle.

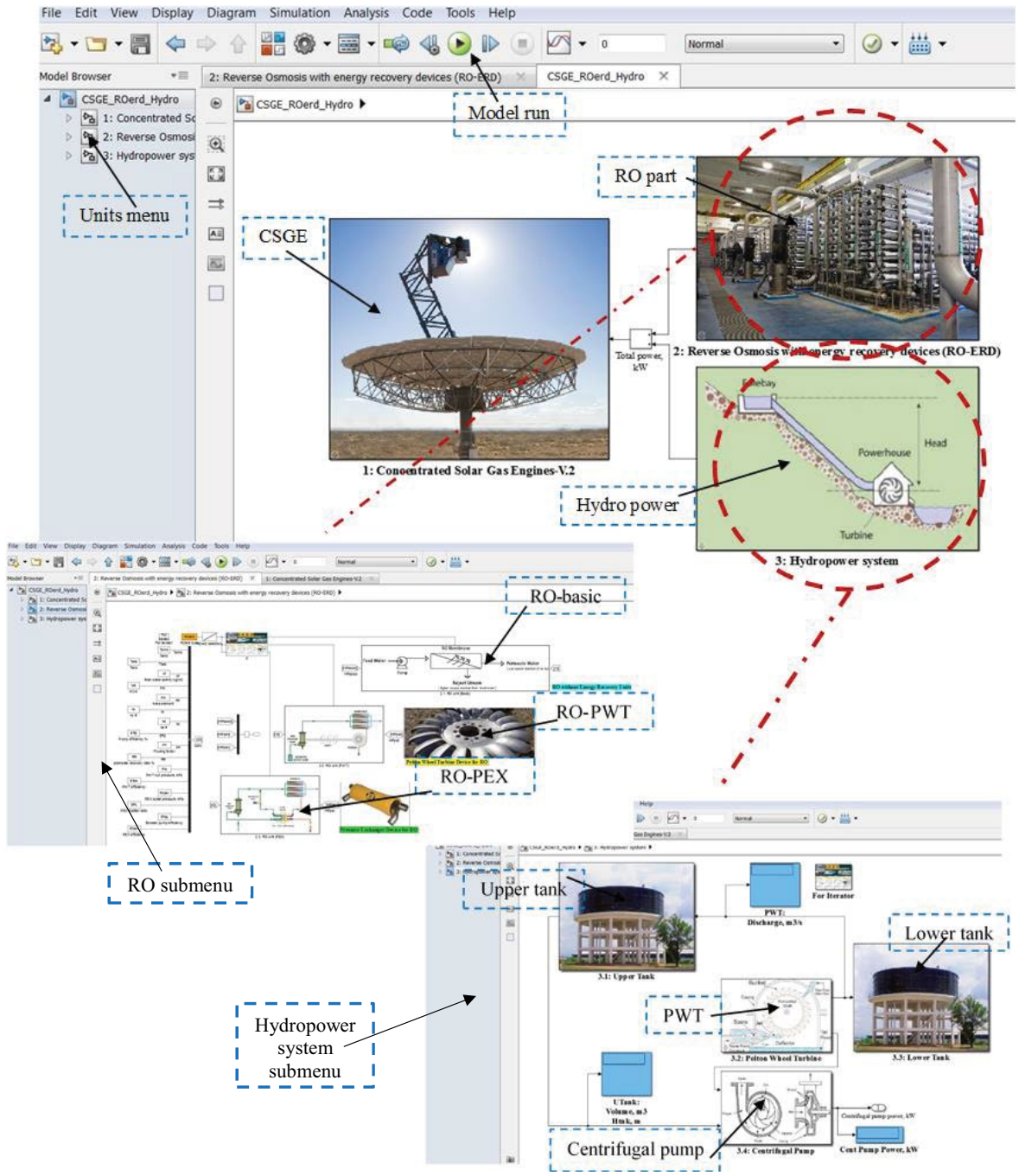

Fig. 4. Proposed system model browser of (CSGE-RO-Hydropower) by the use of REDS program. The system contains CSGE; RO desalination plant block; hydropower system.

the rim angle is 37°. The CSSE mathematical model is presented in Appendix-B part.

3.3. Hydro system optimization

There are many parameters that effects on the performance of hydropower system. One of these parameters is the speed ratio. It is quite important to select a proper speed ratio of hydro PWT because it has a great influence on the power loads, mass flow rate, total head loss, and the hydro efficiency of the system. Also, jet deflection angle parameter has a great influence on the design aspects of the system. Fig. 6 shows the data results of 400 kW hydropower examples based on the effect of speed ratio and jet deflection angle parameters. Fig. 6a shows that increasing the speed ratio up to an optimum value of 0.46 would achieve the maximum hydro efficacy. Meanwhile, the head and power load on the pump will be decreased to its optimum values

Table 6
Specification parameters based on the design technique of modeling concept. RO model [7, 37]

Specified	Calculated
Freshwater productivity, m^3/d	Feed and brine mass flow rates, kg/s
Seawater temperature, °C	Pressure on the HPP, bar
Seawater salinity, ppm	Average pressure, bar
HPP efficiency, %	Product and brine salinities, ppm
Booster pump efficiency, %	Salt rejection percentage, %
Membrane fouling factor, %	HPP power, kW
Number of elements/number of pressure vessels	SPC, kWh/m^3
Element area, m^2	Membranes area, m^2
Recovery ratio, %	
Pressure exchanger (PEX) efficiency, %	
CSGE model [38,40,41]	
Specified	Calculated
Total plant power, kW = RO load	Dish concentration ratio
Stirling engine power, kW = 5–30	Dish area, m^2
Stirling engine No. of cylinders = 4	Receiver area, m^2
Stirling engine piston bore, cm = 5.5–6 [36]	Total plant area, m^2
Stirling engine speed, r.p.m = 1,000–3,500	Dish parabola height, m
	Rim angle ratio
Top cycle temperature, °C = 400–900	Focal length, m
Lower cycle temperature, °C = 25	No. of dishes
Lower cycle pressure, bar = 1.023	Compression ratio
Rim angle = 39°–40° [36]	
	Maximum and minimum specific volumes, m^3/kg
	Top cycle pressure, bar
	Stirling piston volume/cylinder, cm^3
	Stirling piston stroke, cm
	Mean effective pressure, bar
Hydropower model [27,28,43]	
Specified	Calculated
Upper/lower tanks diameter, m	Total system efficiency, %
Power load from RO plant, kW	Hydraulic efficiency, %
PWT_h speed ratio	PWT discharge, m^3/s
Total system head, m	PWT pressure, kPa
Jet diameter/wheel diameter ratio	Jet velocity, m/s
Shaft speed, r.p.m	Peripheral velocity, m/s
Jet deflection angle, degree	Turbine velocity, m/s
Nozzle velocity coefficient	Wheel diameter, m
Mechanical efficiency, %	Number of jets
Shaft speed, r.p.m	Number of buckets
Jet deflection angle, degree	Power load on centrifugal pump, kW
	Pump discharge, m^3/s
	Total pump head, m
	Tubes head losses, m
	Pump pressure, kPa
	Specific speed, rad/s

Table 7
Data results comparison for different energy recovery devices

Parameter	Power, kW	SPC, kWh/m^3	RO ΔP, bar	Power reduction, %
Basic	1,131	7.7	68.66	–
Stages = 9	917.47	6.3	35.8	18–20%
PWT	634	4.35	68.74	43–44%
PEX	380–394	2.704	68.74	60–65%

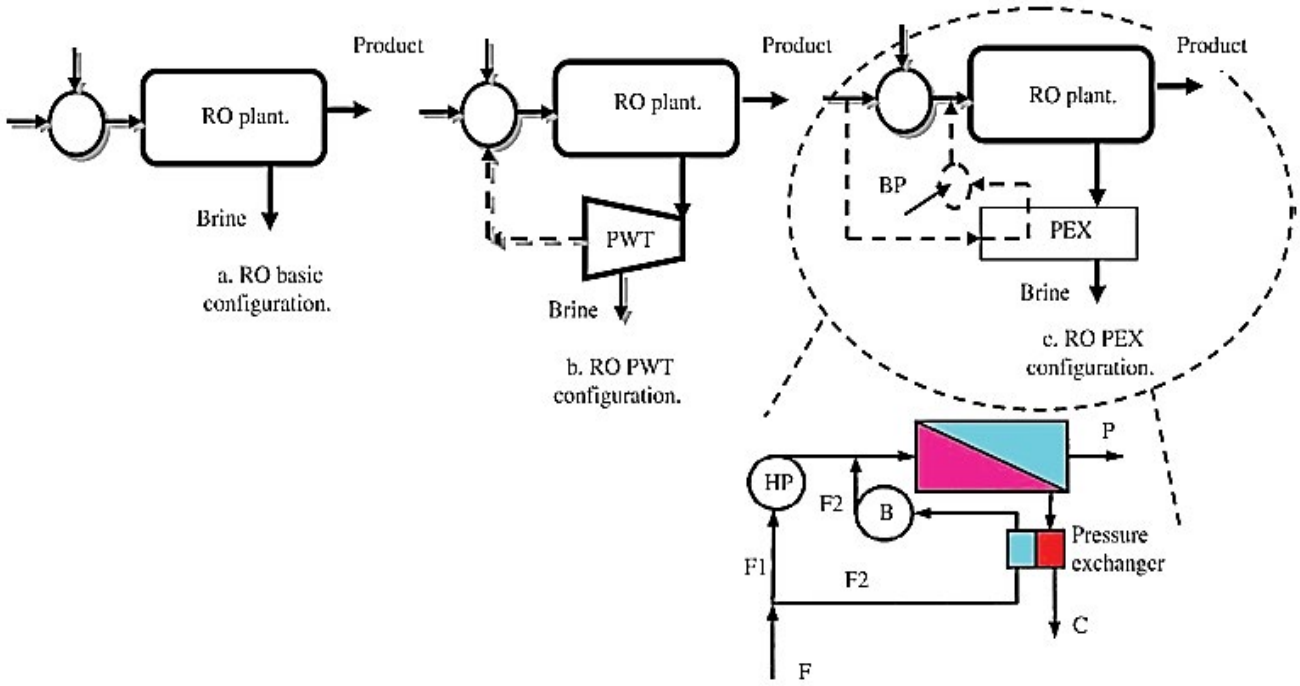

Fig. 5. Schematic draw of the three main configurations of the RO plant: basic, PWT, PEX [7,39]: F, feed, P, product, B, booster pump, HP, high pressure pump.

which are 400 m and 430 kW, respectively (Figs. 6b and c). The same behavior is also noticed in Figs. 6d–f based on the effect of jet deflection angle. Increasing the jet deflection angle would increase the hydropower efficiency (Fig. 6d) and increasing the pump's head and power load (Figs. 6e and f). It is quite clear from Fig. 6 that the best option for speed ratio parameter is at the value of 0.46 and jet deflection angle at 165°. Appendix-C shows the mathematical model of the hydropower plant.

3.4. General assumptions

Based on the optimized design and operating conditions aspects, the following assumptions have been considered:

- Design modeling technique is considered for design aspect discovering.
- Dynamic modeling technique with respect to time period is performed.
- Total water price (TWP, \$/m^3) will be considered the main regulator of this study.
- Solar operating hours = 12 h.
- Hydro operating hours = 12 h.
- For reverse osmosis (RO) part:
  - Optimization results for RO part is considered for productivity range from 3,500 m^3/d up to 10,000 m^3/d.
  - Optimizing the RO will take place first in order to reduce the costs and loads on the CSSE and hydropower plant.
  - Membrane type = BW30-4040
  - Average temperature = 25°C.
  - Recovery ratio = 30%–40%.
  - Pumps efficiency = 85%.
  - Product salinity = 50–150 ppm.
  - Direct capital costs = 1,000 \$/m^3/d.
  - Interest rate = 5%.
  - Membrane purchase costs = 6% of capital costs.
  - Specific labor, chemical costs = 0.05 and 0.033 [8,9].
  - Load factor = 85%
  - Membranes replacement percentage = 15% [8,9].
  - Feed salinity = 1.5 g/m^3 (1,500 ppm).
  - Plant life time = 25 y.

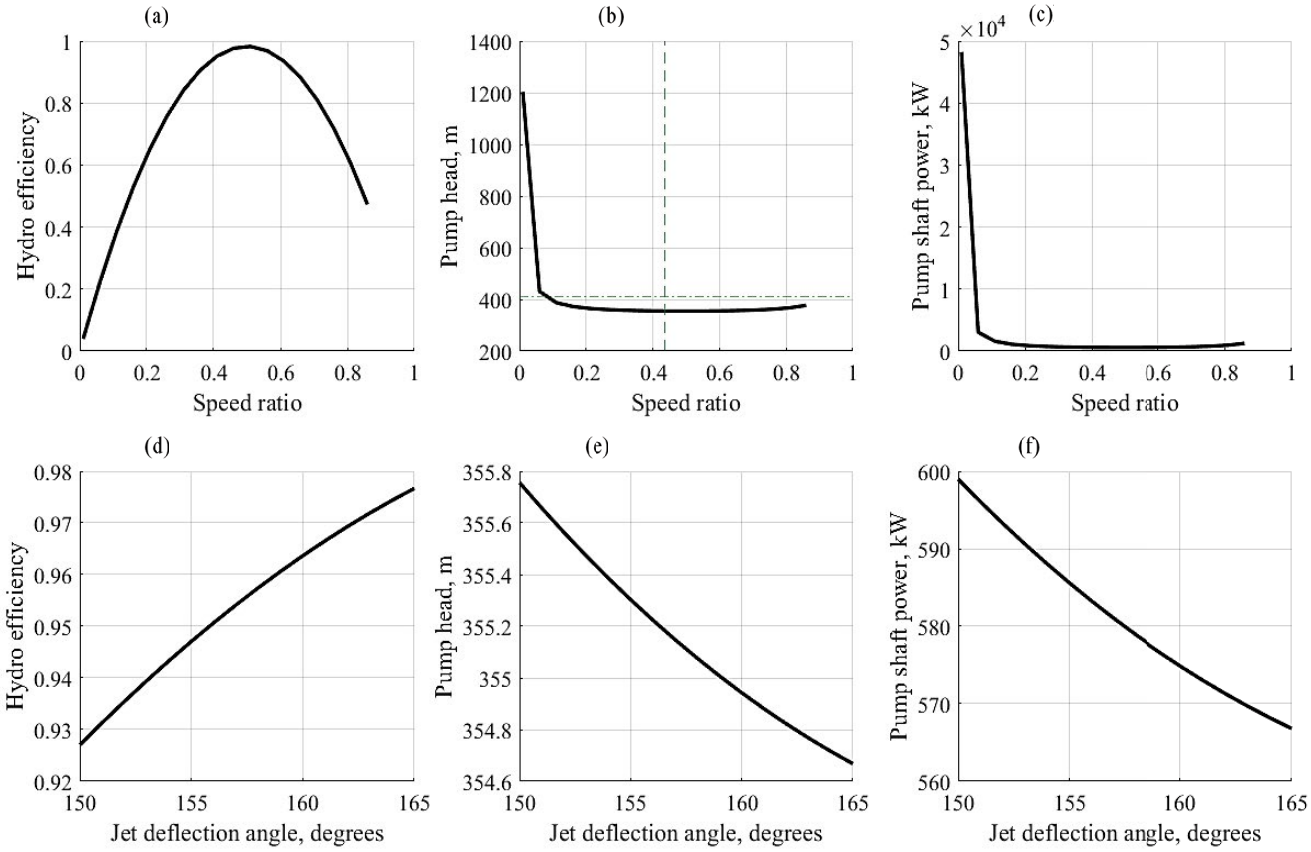

Fig. 6. Effect of speed ratio and jet deflection angle on the design and performance parameters of the hydropower system. (a and d) Hydro efficiency, (b and e) pump head, m, and (c and f) pump power, kW.

- For CSSE part:
  - The top and bottoming temperatures ranges for CSSE are specified as 400°C–800°C for the top range and 25°C for the bottom [34].
  - Engine power = 30 kW.
  - CO_2 is used as main working fluid.
  - Rim angle = 37° [34].
  - Generator efficiency, receiver efficiency, mirror efficiency = 95%, 85%, and 97%.
  - Receiver absorptivity = 94%.
  - Cost of dish, receiver, engine, site, indirect cost, operating and maintenance costs = 300$/m^2, 185$/kW, 400$/kW, 2.2$/m^2, 13%, 37$/kWy [34].
- For operating condition part:
  - For solar radiation and due to the low thermal inertia, a dish Stirling system reacts very quickly on changes in solar thermal input. Thus, steady-state operation is achieved within a few minutes after system start. It can be realized [37] that a dish Stirling system already starts net electric energy production when direct beam insolation (DNI) reaches values around 200–300 W/m^2 (DNI) in the morning, depending on mechanical and thermal losses of the engine as well as the optical performance of the concentrator.
  - 1,000 W/m^2 is assumed for this study in order to fix the dish area (lowering the initial costs), and maximizing the power output while measuring the compression and pressure ratios [37].
- For hydropower part:
- The total height of total head of 335 m is used form a near plateau to the pond (Fig. 7).
- Hydro Pelton wheel turbine (PWT_h) speed ratio = 0.46–0.5, jet diameter/wheel diameter ratio = 1/9, shaft speed = 500 rpm, and the jet deflection angle = 165°.
- Centrifugal pump efficiency = 85%, with speed of 3,600 rpm.
- Centrifugal pump load, kW, would be generated from CSSE solar field. The load power from RO high-pressure pump would be responsible from the Pelton wheel hydro turbine (PWT_h) and the total hydropower plant-specific cost = 4,000 $/kW [38].

4. Results and comments

It is become very hard to recognize the main cause of the effect on the TWP, $/m^3 for the studied system. However, optimizing the RO part would affect the rest of power sources such as CSSE and/or Hydropower plant. Therefore, reducing the load consumption on the RO high pressure pump would reduce all design aspects on solar hydro part, that is, reducing the cost. To minimize the TWP, $/m^3, it is very important to decrease the power load by the RO high

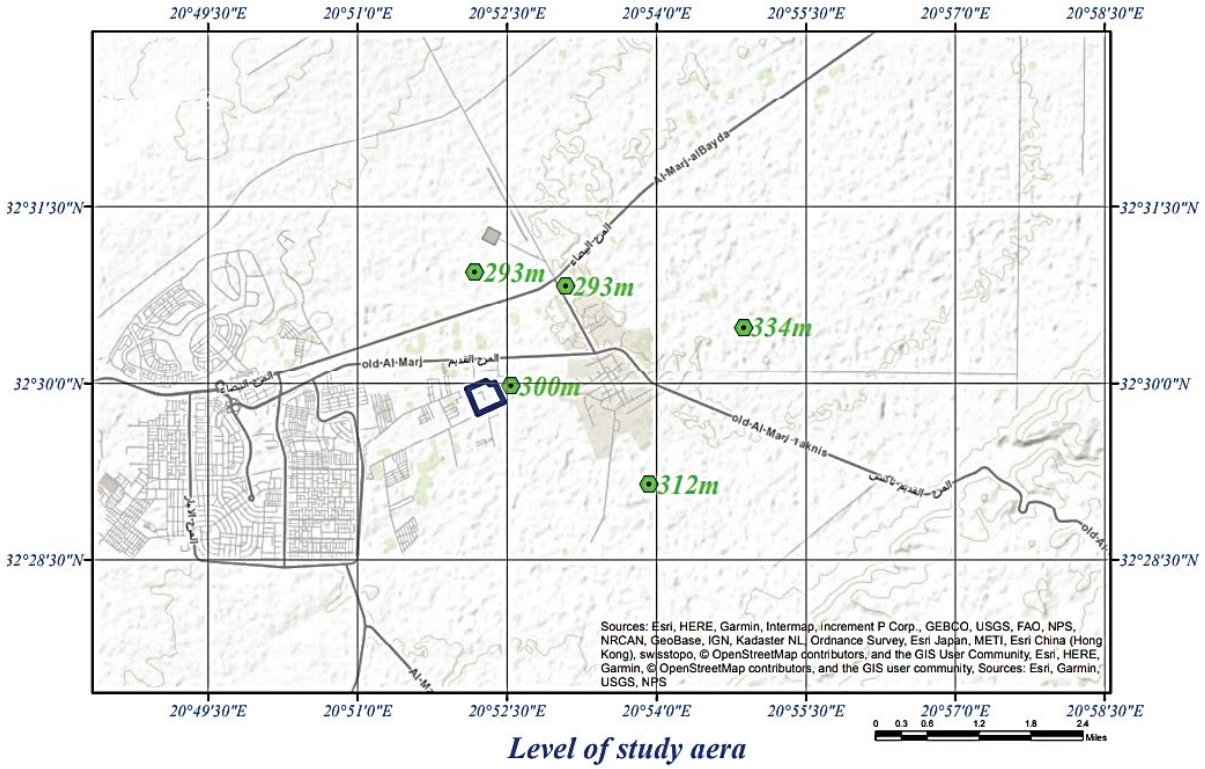

Fig. 7. Site elevation that been used as a head power for hydropower plant.

pressure pump (HPP) with the same freshwater production rate. Fig. 8 shows the data results for the optimized system. Fig. 8 shows the variation of some design parameters based on the variation of total system productivity and load distribution ratio between full loads of solar power and hydropower too. It will become clear to the designer to select between both solar (load ratio = 1), hydro (load ratio = 0), or both in operational case for RO operation. Fig. 8a shows that increasing the total productivity would increase the total system load on the RO pump. The load was varying between 300 kW at 3,500 m^3/d and 1,000 kW at 10,000 m^3/d. It is obvious that the system productivity has a great influence in the total system power, kW. Fig. 8b shows the effect of productivity on hydropower discharge flow. It is quite clear from Fig. 8b that increasing productivity would increase the discharge flow rate. At load ratio = 0, the system will run on fully hydropower with varying discharge values equal to 0.123 m^3/s at 3,500 m^3/d up to 0.351 m^3/s at 10,000 m^3/d. Figs. 8c and d shows the effect of system productivity on solar area for both configurations. Significantly, increasing the productivity and the load ratio up to 1 (100% solar) means increasing the CSSE area in case of solar operation. It is obvious from Figs. 8c and d that the solar filed area would increase by the increasing of load ratio and system productivity and the variation is between 500 m^2 up to 3,500 m^2 at full load on CSGE system.

Fig. 9 shows the effect of total system productivity and load ratio on the total water price (TWP, \$/m^3 Appendix-D) indicator. It is obvious that the increasing of the system productivity has a slight effect on the TWP, \$/m^3. It can cause an increase behavior in water price with a little bit significant change. Changing the load ratio has a great effect on the system TWP, \$/m^3. Increasing the load ratio will lead to fully load on solar part which means lower TWP values. However, it may not serve the system during the night operational periods. For fully operational load on hydropower part, the TWP was recorded about 0.7 \$/m^3. For fully solar power operation, the TWP was in the range of 0.6–0.66 \$/m^3. It is recommended to operate the system on partial load (5,000 m^3/d or load ratio = 60%) in order to reduce the TWP and the CSSE area as well. Table 8 summarizes the data design results for the proposed system related to three cases of productivity (3,500; 5,000; and 10,000 m^3/d).

It is noticed from Table 8 that at 5,000 m^3/d the number of membranes were 336 with total area equal to 2,419.2 m^2. The high pressure pump power was 524 vs. 353 kW and 1,011 kW for 3,500 and 10,000 m^3/d, respectively. The SPC, kWh/m^3 was in range of 2.4–2.5 kWh/m^3. The product salinity was the same for the three cases. As expected, the total solar field area has increase from 875 m^2 at 3,500 m^3/d up to 2,501 m^2 at 10,000 m^3/d case. The total number of dishes was 14, 21, and 39 for 3,500; 5,000; and 10,000 m^3/d, respectively. Engine design parameters are also listed in Table 8. For hydropower part, the system efficiency was recorded as 86.7%, and the average flow discharge was 0.055 m^3/s with jet flow velocity equal to 79.45 m/s. The centrifugal pump power range was 146.2 kW at 33,500 m^3/d, 218.3 at 5,000 m^3/d, and 430 at 10,000 m^3/d. The cost part in Table 8 shows that 3,500 m^3/d case is recorded lower among the rest as anticipated due to the effect of lower solar field area. In general, the 3,500 m^3/d case study is considered lower in cost and design aspects, however, 5,000 m^3/d will be considered an

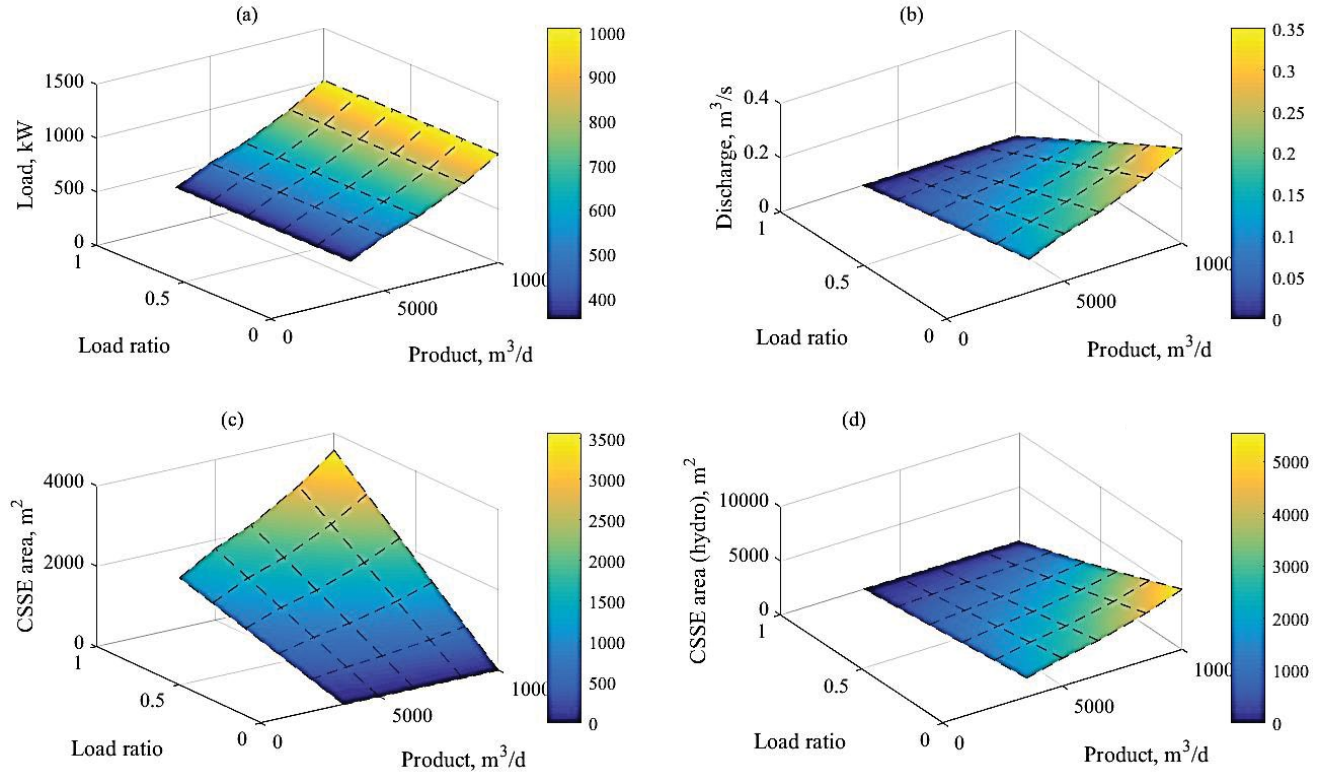

Fig. 8. Optimized data results based on the change in load distribution and system productivity. (a) Load power, kW, (b) hydro discharge, m^3/s, (c) solar CSSE area, m^2, and (d) CSSE area for hydro part, m^2.

intermediate case that should be considered as a normal operating conditions for the system.

Based on results of Fig. 9, it was very clear to consider a load ratio of 70% between CSSE and hydropower concepts. TWP, $\$/m^3$ for all cases was in the range of 0.65 to 0.67. Although the productivity demand has increased from 3,500 up to 10,000 m^3/d, but the range of TWP, $\$/m^3$ was still in same range because of the gain difference is 6,500 m^3/d to be delivered to the user. It is also anticipated from results that the productivity will increase the area of the solar field. Therefore, it is highly recommended to the officials or designers not to consider the area limitations scenario, but the cost limitations scenario because the area is available in such districts (deserts or open plateau).

Fig. 10 shows the effect of productivity range effect on total solar field area and total number of dishes required. Increasing the system productivity would increase the total CSSE area. For instance, at productivity of 6,000 m^3/d, the total solar field area was about 2,500 m^2. Furthermore, at 10,000 m^3/d the total solar field area was about 4,000 m^2. The same behavior has been noticed on the number of dishes parameter. At 10,000 m^3/d, the number of dishes was 40. However, at 3,500 m^3/d, the number of dishes was 15. That's reflecting the system volume based on the total plant productivity.

Fig. 11 shows the change in operating conditions, which represented as input dynamic signals to the proposed system. Fig. 11 simulates a real operational day of the system as a dynamic modeling. The main input signals are the CSGE load, hydropower load, solar radiation, productivity, and number of pressure vessels. It is assumed that the load ratio is varied between (0) and (1) values depending on the variation of solar radiation. For example, in case of no existence of solar radiation, the load signal for CSGE will be turned to (0), however, the value of (1) will be considered for hydropower system. Thence, the productivity parameter will take the value of 3,500 m^3/d and the number of pressure vessels will take the value of (35). Such condition will be continue during the day off periods (no existence of solar radiation) 12:00 a.m. until 9:00 a.m. After that, the solar radiation value will gradually increase until fixing at DNI = 1,000 W/m^2.

In such case, load signal on hydropower system will take the value of (0) and the CSGE will take the value of (1) based on load ratio. Meanwhile, the productivity range will gradually increase until reaching its maximum value (10,000 m^3/d). Moreover, the number of pressure vessels will take the signal value of 100 according to the productivity change. Such effect of the signals will continue constant from 9:00 a.m. until 18:00 p.m. Meanwhile, the solar radiation signal will continue in gradual decreasing until reaching the day off value (0), and the CSGE load will take the same value as well. Thence, the system will continue in operational case depending on hydropower system from 19:00 p.m. until 9:00 a.m.

Figs. 11a–f show the data results based on the dynamic variation of the design operating conditions that been considered in the assumptions. Fig. 11a shows the dynamic change in specific power consumption (SPC, kWh/m^3).

Table 8
Data results for the system at 3,500; 5,000; 10,000 m^3/d and load ratio = 70% case study

RO with pressure exchanger model			
	3,500	5,000	10,000
Feed/brine mass flow rates, m^3/h	486.1/340.3	694.4/486.1	1,389/972.2
Pressure on the HPP, bar	65.73	68.41	65.73
Product/brine salinities, ppm	1.45/2,000.2	1.39/2,000.18	1.45/2,000.187
Salt rejection percentage, %	99.9	99.9	99.9
HPP power, kW	353.7	524.4	1,011
SPC, kWh/m^3	2.452	2.517	2.425
Membranes area, m^2	7.2 × 7 × 35	7.2 × 7 × 48	7.2 × 7 × 100
CSGE model (CO_2 working gas)			
Dish concentration ratio	1,598		
Dish area, m^2	106.1		
Receiver area, m^2	0.06635		
Total plant area, m^2	875.2 + 516.7	1,298 + 771.7	2,501 + 1,520
Dish parabola height, m	1		
Rim angle ratio	0.72		
Focal length, m	8.367		
No. of dishes	9 + 5	13 + 8	24 + 15
Compression ratio	11.24		
Mean effective pressure, bar	14.4		
Max/Min specific volumes, m^3/kg	0.5506/0.049		
Top cycle pressure, bar	41.38		
Stirling piston volume/cylinder, cm^3	58.84		
Stirling piston stroke, cm	2.477		
Hydropower model			
Total system efficiency, %	86.73		
Hydraulic efficiency, %	96.36		
PWT discharge, m^3/s	0.03723	0.05519	0.1064
PWT pressure, kPa	32.86		
Jet velocity, m/s	79.45		
Peripheral velocity, m/s	36.55		
Turbine velocity, m/s	0.02168	0.0264	0.03664
Wheel diameter, m	1.4	1.396	1.396
Number of buckets	19.5–20		
Power load on centrifugal pump, kW	146.2	218.3	430
Pump discharge, m^3/s	0.03723	0.05519	0.1064
Total pump head, m	340.2	342.7	350
Tubes head losses, m	0.5331	0.5256	0.5181
Pump pressure, kPa	3,337	3,362	3,433
Cost results			
Membranes costs, $	2.1e6	3e6	6e6
Annual replacement costs, $/y	3.15e5	4.5e5	9e5
Annual fixed charges, $/y	2.483e5	3.548e5	7.095e5
Annual chemical costs, $/y	3.583e4	5.119e4	1.024e5
Annual labor costs, $/y	5.429e4	7.756e4	1.551e5
Annual CSSE costs, $/y	2.485e4	3.446e4	6.212e4
Annual hydropower costs, $/y	3.011e4	4.465e4	8.604e4
TWP, $/m^3$	0.6524	0.6628	0.6795

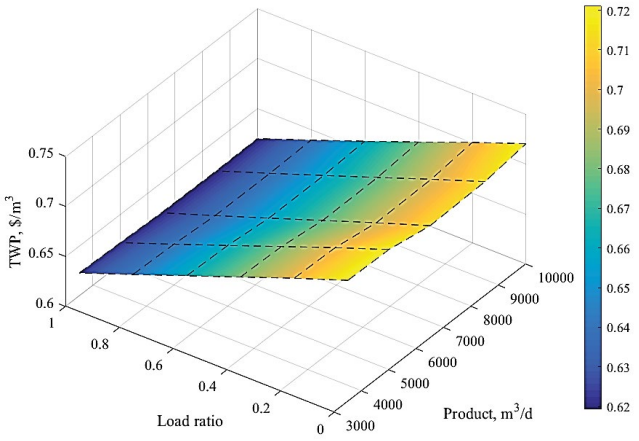

Fig. 9. Data results for TWP, $/m^3 based on the variation of system productivity and load ratio.

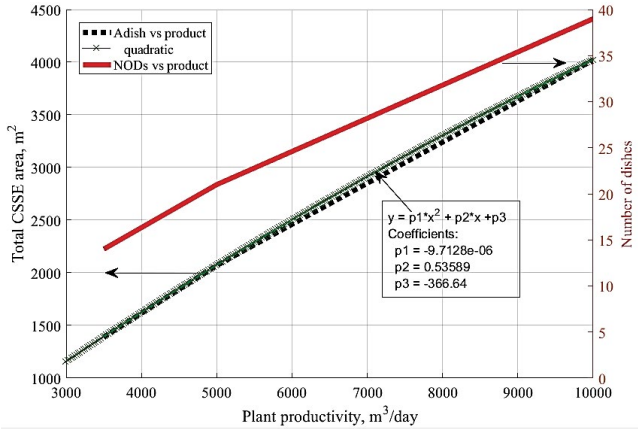

Fig. 10. Effect of total plant productivity on the CSSE total area and number of dishes.

It shows that the range was around 2–4 kWh/m^3. At the beginning, the RO load will be responsible from hydropower at nearly 1/3 of the total load on RO pump. After that, along the solar periods, CSSE will take the full effect beside the CSSE used for centrifugal pump. Figs. 11b–d show the RO pressure, exergy destruction rate, kW, and load demanded by the RO pump. It is obvious on Fig. 11b that the productivity change has a large effect on the RO pressure. The pressure was varying from 40 bar up to 100 bar depending on lower and upper cases. The same effect was noticed in Figs. 11c and d because of the large feed consumption through the RO pump. Fig. 11e shows the variation of loads on CSSE and hydropower parts. The diagram shows the differences of the load distribution between both power systems (solar and hydro).

As the solar field operates, the hydroelectric turbine stops rotating. While the hydroelectric actuator is operating (about a third of the energy), the solar field stops working. All of this is related to changing the impact of solar energy throughout the day, as in the dynamic case. Fig. 11f shows the variation in hydro PWT unit based on discharge flow rate, m^3/s. The results reveal that solar hydro should be operated at minimum load requirements in order to reduce the TWP, $/m^3 (Appendix-D), and SPC, kWh/m^3 parameters. Load distribution ratio should be in the range of 0.6–0.7. The load on the hydropower should be minimized by the use of pressure exchanger unit with RO desalination plant.

5. Conclusion

Membrane technology such as reverse osmosis is playing an increasingly important role in the reclamation of municipal wastewater. Due to the growing demand for high quality water in urban areas, purification of wastewater became one of the preferred means of augmenting water resources. A case study in Al-Marj city, Libya is presented in this work. The aim of this study was to transform the location of industrial wastewater sewage pond (1,065,625 m^3) into a permanent supply of freshwater by the aid of reverse osmosis technology. The water and soil analyses in the mentioned location showed a negative impact on the environment. Therefore, it is becoming urgent to recycle the city sewage pond and produce freshwater for 55,000–100,000 inhabitants. Instead of using conventional sources of power, solar energy via CSSE and hydropower have been used in this study for that purpose. The main reason of using solar and hydropower energies is that the location of operation has a great potential of solar energy and has large plateau area over 400 m from the sea level which is considered a head power for the hydro turbine unit.

CSGE has a great stability along the day regarding to the AC current provided for the reverse osmosis high-pressure pump. Based on previous studies by the authors, CSSE with CO_2 gas is considered in this work. During the sun-off periods, hydropower system is used as an alternative source of power considering the use of environmental plateau (level = 340–400 m) and geographical benefits of the location of operation. Based on the analysis performed in this work, the following conclusions could be withdraw:

- The wastewater sewage pond will be operated as a large water storage tank (1,065,625 m^3) by supplying the RO plant.
- The RO load was varying according to the total productivity range (3,500–10,000 m^3/d), that is, the load was varying between 400 and 1,200 kW.
- The hydropower turbine speed ratio should be in the range of 0.4–0.5.
- It is anticipated from the system to produce an amount of 10,000 m^3/d of freshwater.
- Pressure exchanger configuration is recommended for the RO in order to reduce the power consumption by 70%.
- The specific power consumption (SPC, kWh/m^3) was varying between 2.5 and 4 kWh/m^3.
- The load on hydropower was not exceeded over 400 kW.
- Total hydro system head is equal to 400 m and the supply tank volume was 1,852 m^3.
- The average solar dish power is 40 kWe and the total CSSE area is around 3,500–4,000 m^2.
- The system total water price (TWP, $/m^3) was in the range of 0.65 $/m^3 and 0.68 $/m^3.

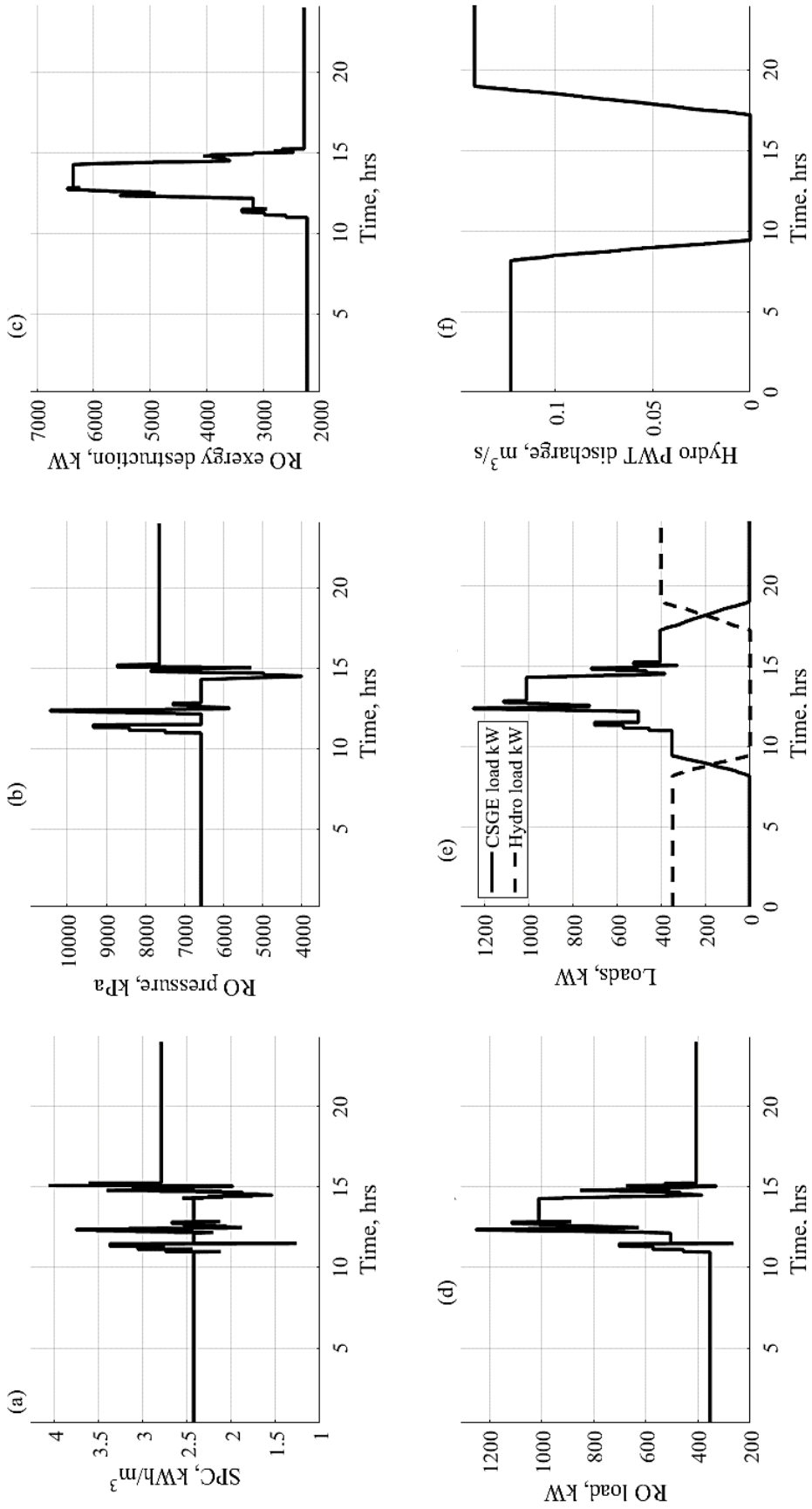

Fig. 11. Data results based on dynamic operating conditions. (a) Specific power consumption, kWh/m3, (b) RO pressure, kPa, (c) exergy destruction rate, kW, (d) RO load, kW, (e) loads on CSSE and hydro, kW, and (f) hydro PWT discharge, m3/s.

In conclusion, it is possible to combine solar energy (concentrated solar dish engine) with hydropower for large scales RO desalination plants, taking into consideration the location space area, elevations, and volume of the supply reservoir.

Symbols

A	—	Area, m^2
A_e	—	Element area, m^2
A_{dish}	—	Dish area, m^2
A_p	—	Piston area, m^2
C_p	—	Specific heat capacity, kJ/kg°C at constant pressure
C_v	—	Specific heat capacity, kJ/kg°C at constant volume
CSBE	—	Concentrated solar Brayton engine
CSSE	—	Concentrated solar Stirling engine
C_t	—	Total cost, $
CP	—	Turbine power coefficient
CR	—	Compression ratio, concentration ratio for the dish
D	—	Diameter, m
DHI	—	Diffuse horizontal irradiance, kWh/m^2
DNI	—	Direct normal irradiance, kWh/m^2
f	—	Focal length, m
FF	—	Fouling factor
GHI	—	Global Horizontal Irradiance, kWh/m^2
HPP	—	High pressure pump
H_{dish}	—	Dish parabola height, m
I_s	—	Solar intensity, W/m^2
k	—	Permeability
L	—	Length, m
M	—	Mass flow rate, m^3/h, kg/s
MEP	—	Mean effective pressure, bar
NOD	—	Number of dishes
n	—	Number, #
N_e	—	RO Element number
N_V	—	Number of pressure vessels
NOB	—	Number of batteries, #
NOC	—	Number of cells, #
NOM	—	Number of modules, #
NWT	—	Number of wind turbines, #
OH	—	Operating hours, h
OM	—	Organic material
P	—	Power, permeator, or pressure, bar
P	—	Pressure, bar
P_{SE}	—	Stirling engine power, kW
P_{total}	—	Total power, kW
ΔP	—	Pressure, bar
Q	—	Discharge, m^3/s
RR	—	Recovery ratio
R	—	Specific gas constant, kJ/kg°C
RA	—	Rim angle, degrees
RAR	—	Rim angle ratio
r.p.m	—	Speed, rev/min
r_p	—	Pressure ratio
SPC	—	Specific power consumption, kWh/m^3
SR	—	Salt rejection
T	—	Temperature, °C
TCF	—	Temperature correction factor
TWP	—	Total water price, $/m^3
V	—	Volume, cm^3
v	—	Specific volume, m^3/kg
W	—	Work, kW
X	—	Salinity, ppm

Subscripts

a	—	Actual
air	—	Ambient
atm	—	Atmospheric
b	—	Brine, battery
c	—	Cell
cent	—	Centrifugal pump
d	—	Distillate product
e	—	Element
EG	—	Electric generator
f	—	Feed
g	—	Gas
h	—	High
i	—	Inlet
l	—	Low
opt	—	Optical
o	—	Out
p	—	Piston
PWT	—	Pelton wheel turbine
RO	—	Reverse osmosis
t	—	Turbine, total
v	—	Vessel
w	—	Water

Greek

η	—	Efficiency, %
Π	—	Osmotic pressure, kPa
ρ	—	Density, kg/m^3
ω	—	Rad/s
γ	—	Isentropic index

References

[1] M. El Bastawesy, S. Adel, I.N.L. Mohamed, Management of waste water discharge within the Nile Valley of Egypt: the collapse of Al Ballanah waste water's lake in Aswan in September 2013, Egypt. J. Remote Sens. Space Sci., 21 (2018) 149–158.

[2] http://www.biologydiscussion.com/ecology/wastewater/wastewater-problem-and-its-treatment-ecology/70914

[3] P. Hoornaert, Reverse Osmosis: EPO Applied Technology Series, v4, 1984, pp. 97–105, ISBN 0-08-031144-X, Pergamon Press Ltd., Headington Hill Hall, Oxford OX3 0BW, England.

[4] V. Barbosa Brião, A.C. Vieira Salla, T. Miorando, M. Hemkemeier, D.P. Cadore Favaretto, Water recovery from dairy rinse water by reverse osmosis: giving value to water and milk solids, Resour. Conserv. Recycl., 140 (2019) 313–323.

[5] Y. Uojima, Operation of reverse osmosis process for industrial waste water reclamation, Desalination, 23 (1977) 87–95.

[6] C.R. Bartels, Reverse Osmosis Membranes Play Key Role in Wastewater Reclamation, 2006, Available at: https://www.waterworld.com/articles/wwi/print/volume-21/issue-6/features/reverse-osmosis-membranes-play-key-role-in-wastewater-reclamation.html

[7] M.A. Sharaf, A.S. Nafey, L. Garcia-Rodriguez, Thermo-economic analysis of a combined solar organic Rankine cycle reverse osmosis desalination process with different energy recovery configurations, Desalination, 261 (2010) 138–147.

[8] M.A. Sharaf Eldean, Design and Simulation of Solar Desalination Systems, Ph.D. Thesis, 2011, Suez Canal University, Faculty of Petroleum & Mining Engineering, Bibliography No.: 11114571.
[9] A.S. Nafey, M.A. Sharaf. Combined solar organic Rankine cycle with reverse osmosis desalination process: energy, exergy, and cost evaluations, Renewable Energy, 35 (2010) 2571–2580.
[10] M.A. Sharaf, Thermo-economic comparisons of different types of solar desalination processes, J. Solar Energy Eng., 134 (2012) 031001.
[11] A.M. Delgado-Torres, L. García-Rodríguez, V.J. Romero-Ternero, Preliminary design of a solar thermal-powered seawater reverse osmosis system, Desalination, 216 (2007) 292–305.
[12] A.M. Delgado-Torres, L. García-Rodríguez, Status of solar thermal driven reverse osmosis desalination, Desalination, 216 (2007) 242–251.
[13] A.M. Delgado-Torres, L. García-Rodríguez, Comparison of solar technologies for driving a desalination system by means of an organic Rankine cycle, Desalination, 216 (2007) 276–291.
[14] E.Sh. Mohamed, G. Papadakis, E. Mathioulakis, V. Belessiotis, A direct coupled photovoltaic seawater reverse osmosis desalination system toward battery based systems-a technical and economical experimental comparative study, Desalination 221 (2008) 17–22.
[15] A.M. Helal, S.A. Al-Malek, E.S. Al-Katheeri, Economic feasibility of alternative designs of a PV-RO desalination unit for remote areas in the United Arab Emirates, Desalination, 221 (2008) 1–16.
[16] D. Manolakos, E.Sh. Mohamed, I. Karagiannis, G. Papadakis, Technical and economic comparison between PV-RO system and RO-Solar Rankine system. Case study: Thirasia Island, Desalination, 221 (2008) 37–46.
[17] G.E. Ahmad, J. Schmid, Feasibility study of brackish water desalination in the Egyptian deserts and rural regions using PV systems, Energy Convers. Manage., 43 (2002) 2641–2649.
[18] E. Tzen, K. Perrakis, P. Baltas, Design of a standalone PV-desalination system for rural areas, Desalination, 119 (1998) 327–334.
[19] A.A. Hossam-Eldin, K.A. Abed, K.H. Youssef, H. Kotb, Techno-economic optimization and new modeling technique of PV-wind-reverse osmosis desalination plant at variable load conditions, Int. J. Environ. Sci. Dev., 10 (2019) 223–230.
[20] C. Ghenai, A. Merabet, T. Salameh, E.C. Pigem, Grid-tied and stand-alone hybrid solar power system for desalination plant, Desalination, 435 (2018) 172–180.
[21] M. Gökçek, Integration of hybrid power (wind-photovoltaic-diesel-battery) and seawater reverse osmosis systems for small-scale desalination applications, Desalination, 435 (2018) 210–220.
[22] M. Laissaoui, P. Palenzuela, M.A. Sharaf Eldean, D. Nehari, D.-C. Alarcón-Padilla, Techno-economic analysis of a stand-alone solar desalination plant at variable load conditions, Appl. Therm. Eng.,133 (2018) 659–670.
[23] Z. Wang, X. Lin, N. Tong, Z. Li, S. Sun, C. Liu, Optimal planning of a 100% renewable energy island supply system based on the integration of a concentrating solar power plant and desalination units, Int. J. Electr. Power Energy Syst., 117 (2020) 105707.
[24] N. Mousavi, G. Kothapalli, D. Habibi, M. Khiadani, C.K. Das, An improved mathematical model for a pumped hydro storage system considering electrical, mechanical, and hydraulic losses, Appl. Energy, 247 (2019) 228–236.
[25] H. Zhang, Z. Lu, W. Hu, Y. Wang, L. Dong, J. Zhang, Coordinated optimal operation of hydro–wind–solar integrated systems, Appl. Energy, 242 (2019) 883–896.
[26] Z. Liu, Z. Zhang, R. Zhuo, X. Wang, Optimal operation of independent regional power grid with multiple windsolar-hydro-battery power, Appl. Energy, 235 (2019) 1541–1550.
[27] S. Camal, F. Teng, A. Michiorri, G. Kariniotakis, L. Badesa, Scenario generation of aggregated wind, photovoltaics and small hydro production for power systems applications, Appl. Energy, 242 (2019) 1396–1406.
[28] A.S. Kocaman, V.Modi, Value of pumped hydro storage in a hybrid energy generation and allocation system, Appl. Energy, 205 (2017) 1202–1215.
[29] S. Han, L.-na. Zhang, Y.-q. Liu, H. Zhang, J. Yan, L. Li, X.-h. Lei, X. Wang, Quantitative evaluation method for the complementarity of wind–solar–hydro power and optimization of wind–solar ratio, Appl. Energy, 236 (2019) 973–984.
[30] A.S. Nafey, M.A. Sharaf, L. Garcia-Rodriguez, A new visual library for design and simulation of solar desalination systems (SDS), Desalination, 259 (2010) 197–207.
[31] M.A. Sharaf Eldean, A.M. Soliman, A new visual library for modeling and simulation of renewable energy desalination systems (REDS), Desal. Water Treat., 51 (2013) 6905–6920.
[32] https://globalsolaratlas.info/?c=22.828248,23.176858,5&s=26.818689,20.291559
[33] https://www.redslibrary.com/product-page/solar-radiation-model
[34] M.A. Sharaf Eldean, K.M. Rafi, A.M. Soliman, Performance analysis of different working gases for concentrated solar gas engines: Stirling & Brayton, Energy Convers. Manage., 150 (2017) 651–668.
[35] V. Siva Reddy, S.C. Kaushik, S.K. Tyagi, Exergetic analysis and performance evaluation of parabolic dish Stirling engine solar power plant, Int. J. Energy Res., 37 (2013) 1287–1301.
[36] A.Z. Hafez, A. Soliman, K.A. El-Metwally, I.M. Ismail, Solar parabolic dish Stirling engine system design, simulation, and thermal analysis, Energy Convers. Manage., 126 (2016) 60–75.
[37] K. Lovegrove, W. Stein, Concentrating Solar Power Technology, Principles, Developments and Applications, 1st ed., Woodhead Publishing, 19th October 2012, ISBN: 9780857096173.
[38] Renewable Energy Technologies: Cost Analysis Series, Vol. 1, International Renewable Energy Agency IRENA, Available at: https://www.irena.org//media/Files/IRENA/Agency/Publication/2018/Jan/IRENA_2017_Power_Costs_2018.pdf
[39] W. Mark, B. Craig, Optimization of seawater RO systems design, Desalination, 173 (2005) 1–12.
[40] H.T. El-Dessouky, H.M. Ettouney, Fundamentals of Salt Water Desalination, Elsevier Science, 20th March 2002, ISBN: 9780080532127.
[41] B. Kongtragool, S. Wongwises, A review of solar-powered Stirling engines and low temperature differential Stirling engines, Renewable Sustainable Energy Rev., 7 (2003) 131–154.
[42] P.K. Nag, Basic and Applied Thermodynamics, ISBN: 0–07–047338–2, Tata McGraw-Hill, New Delhi, 2002.
[43] A.M.A. Al-Dafaie, M.-E. Dahdolan, M.A. Al-Nimr, Utilizing the heat rejected from a solar dish Stirling engine in potable water production, Solar Energy, 136 (2016) 317–326.
[44] J.A. Duffie, W.A. Beckman, Solar Engineering of Thermal Processes, John Wiley & Sons Inc., Hoboken, NJ, 2013.
[45] P.R. Fraser, Stirling Dish System Performance Prediction Model, M.Sc. Thesis, University of Wisconsin-Madison, Madison, 2008.
[46] Z. Husain, Mohd.Z. Abdullah, Z. Alimuddin, Basic Fluid Mechanics and Hydraulic Machines, ISBN: 978-81-7800-148-7, 2008.
[47] Higher Institute of Agricultural Techniques, Al-Marj, Libya, Available at: https://1742268.site123.me

Appendix-A: RO mathematical model

The mathematical model for the proposed RO unit is written as follows [7,40]:

The feed flow rate M_f based on recovery ratio RR and distillate flow rate M_d is:

$$M_f = \frac{M_d}{\mathrm{RR}} \tag{1}$$

The distillate product salt concentration X_d:

$$X_d = X_f \times \left(1 - \mathrm{SR}\right) \tag{2}$$

where X_f is the feed flow rate salt concentration, and SR is the salt rejection percentage; and the rejected brine is found from:

$$M_b = M_f - M_d \tag{3}$$

The rejected salt concentration kg/m^3 is estimated by:

$$X_b = \frac{M_f \times X_f - M_d \times X_d}{M_b} \tag{4}$$

The average salt concentration kg/m^3 is estimated as:

$$X_{\mathrm{av}} = \frac{M_f \times X_f + M_b \times X_b}{M_f + M_b} \tag{5}$$

The temperature correction factor TCF is found by the relation below:

$$\mathrm{TCF} = \exp\left(2{,}700 \times \left(\frac{1}{273+t} - \frac{1}{298}\right)\right) \tag{6}$$

The membrane water permeability k_w:

$$k_w = 6.84 \times 10^{-8} \times \frac{\left(18.6865 - \left(0.177 \times X_b\right)\right)}{\left(t + 273\right)} \tag{7}$$

The salt permeability k_s is:

$$k_s = \mathrm{FF} \times \mathrm{TCF} \times 4.72 \times 10^{-7} \times \left(0.06201 - \left(5.31 \times 10^{-5} \times \left(t + 273\right)\right)\right) \tag{8}$$

where FF is the membrane-fouling factor. The calculations of osmotic pressure for feed side, brine side, and distillate product side are found as follows:

$$\prod_f = 75.84 \times X_f \tag{9}$$

$$\prod_b = 75.84 \times X_b \tag{10}$$

$$\prod_d = 75.84 \times X_d \tag{11}$$

The average osmotic pressure on the feed side:

$$\prod_{\mathrm{av}} = 0.5 \times \left(\prod_f + \prod_b\right) \tag{12}$$

The net osmotic pressure across the membrane:

$$\Delta\prod = \prod_{\mathrm{av}} - \prod_d \tag{13}$$

The net pressure difference across the membrane:

$$\Delta P = \left(\frac{M_d}{3{,}600 \times \mathrm{TCF} \times \mathrm{FF} \times A_e \times N_e \times N_v \times k_w}\right) + \Delta\prod \tag{14}$$

where A_e is the element area in m^2, n_e is number of membrane elements, and N_v is the number of pressure vessels. The required power input in kW for the RO high-pressure pump (HPP) is estimated as:

$$\mathrm{HPP}_{\mathrm{power}} = \frac{1{,}000 \times M_f \times \Delta P}{3{,}600 \times \rho_f \times \eta_p} \tag{15}$$

Where ρ_f is the feed flow rate density, and η_p is the driving pump mechanical efficiency. The specific power consumption in kWh/m^3 is estimated as:

$$\mathrm{SPC} = \frac{\mathrm{HPP}_{\mathrm{power}}}{M_d} \tag{16}$$

Appendix-B: CSSE mathematical model

The solar powered gas engine system uses a large parabolic a mirror to focus the sun rays on the hot side of a gas engine. The reflective mirrors are mounted on a parabolic-shaped structure using stamped sheet metal. Other structure accessories are constructed of steel. The good solar dish reflectors must have the following properties; reasonable weight; hardness against deflection and wind load, durability against moisture and temperature changes; parts must be flexible; low cost, effective reflecting materials; and long lifetime [36]. The following equations are representing the dish calculation model. By assigning the total plant power and the engine power, the total number of the plant dishes is calculated.

$$\mathrm{NOD} = \frac{P_{\mathrm{total}}}{P_{\mathrm{SE}}} \tag{17}$$

The actual Stirling engine efficiency is calculated from the following equation [41–43]:

$$\eta_{\mathrm{SE}} = 0.5 \times \left(1 - \frac{T_l}{T_h}\right) \tag{18}$$

The Stirling engine volume ratio (compression ratio) based on the efficiency is obtained as follows [41]:

$$\tau = \frac{T_h}{T_l} \tag{19}$$

$$\Theta = \frac{\frac{1 - \left(1/\tau\right)}{\eta_{\mathrm{SE}}} - 1}{1 - \left(1/\tau\right)} \tag{20}$$

$$\mathrm{CR}_{\mathrm{SE}} = e^{\left(\frac{C_v}{R\times\Theta}\right)} \tag{21}$$

where, C_v is the specific heat capacity of the gas at constant volume, kJ/kg°C, and R is the specific gas constant, kJ/kg°C. The Stirling pressure ratio is then calculated by the calculating of the top cycle pressure:

$$P_h = P_l \times \mathrm{CR}_{\mathrm{SE}} \times \frac{T_h}{T_l} \tag{22}$$

The pressure ratio is then calculated:

$$r_{p_{\mathrm{SE}}} = \frac{P_h}{P_l} \tag{23}$$

The total plant efficiency is obtained by the assigning generator efficiency and optical and receiver efficiencies:

$$\eta_{\mathrm{total}} = \eta_{\mathrm{SE}} \times \eta_{\mathrm{EG}} \times \eta_{\mathrm{rec}} \times \eta_{\mathrm{opt}} \tag{24}$$

Dish mirror area, m²:

$$A_{\mathrm{dish}} = \frac{P_{\mathrm{SE}}}{I_s \times \eta_{\mathrm{total}}} \tag{25}$$

where I_s is the solar radiation, W/m². Rim angle ratio (RAR) is calculated from the following sequence [42]:

$$\mathrm{RAR} = 1.003 \times e^{-\left(\frac{\mathrm{RA}-11.28}{13.86}\right)^2} + 2.186 \times e^{-\left(\frac{\mathrm{RA}+100.2}{127.6}\right)^2} \tag{26}$$

where RA is the rim angle in degree. The dish focal length f is calculated in m:

$$f = \mathrm{RAR} \times D_{\mathrm{dish}} \tag{27}$$

The dish parabola height, m [39]:

$$H_{\mathrm{dish}} = \frac{D_{\mathrm{dish}}^2}{16 \times f} \tag{28}$$

The calculations of the dish concentration ratio CR = A_{dish}/A_{rec} [43–45] is obtained through the following sequence:

$$\psi = \left(\frac{T_{\mathrm{amb}}}{T_h}\right)\left(\frac{1}{5\times T_h^4 - T_{\mathrm{amb}}^4 + 4\times T_h^3}\right) \tag{29}$$

$$\mathrm{CR}_{\mathrm{dish}} = \frac{\sigma = 5.669e^{-8}}{0.9 \times \alpha_{\mathrm{rec}} \times \mathrm{Is} \times \psi} \tag{30}$$

Then the receiver area, m² is calculated:

$$A_{\mathrm{rec}} = \frac{A_{\mathrm{dish}}}{\mathrm{CR}_{\mathrm{dish}}} \tag{31}$$

The total plant surface area, m²:

$$A_{\mathrm{total}} = A_{\mathrm{dish}} \times \mathrm{NOD} \tag{32}$$

The mean effective pressure is calculated as follows [41]:

$$\mathrm{MEP} = \frac{P_{\mathrm{atm}} \times \left(\mathrm{CR}_{\mathrm{SE}} + 1\right)\left(\tau + 1\right)}{4} \tag{33}$$

Therefore, the Stirling engine piston dimensions is calculated [41]:

The piston volume, cm³:

$$V_p = \frac{60 \times P_{\mathrm{SE}}}{4\pi \times \mathrm{NOC} \times \mathrm{MEP} \times \mathrm{r.p.m} \times F \times \frac{T_h - T_l}{T_h + T_l}} \tag{34}$$

where NOC is the number of cylinders, and the F parameter is equal to 0.25–0.35 [41]. The stroke, cm:

$$\mathrm{Stroke} = \frac{V_p}{A_p} \tag{35}$$

Appendix-C: Hydropower cycle mathematical model

The main hydropower cycle consists of upper tank, Pelton Wheel drive turbine, centrifugal pump, and lower tank.

C.1. Pelton wheel drive model [30,31,46]:

The hydraulic efficiency is determined based on the speed ratio (SR) and deflection angle (θ):

$$\eta_{\mathrm{hyd}} = 2 \times \mathrm{SR} \times \left(1 - \mathrm{SR}\right) \times \left(1 - \cos d\left(\theta\right)\right) \tag{36}$$

The total efficiency based on hydraulic and mechanical efficiencies is then calculated:

$$\eta_{\mathrm{total}} = \eta_{\mathrm{mech}} \times \eta_{\mathrm{hyd}} \tag{37}$$

The jet velocity V_j, m/s is calculated total head H_t, and velocity coefficient (CV):

$$V_j = \mathrm{CV} \times \sqrt{\left(2g \times H_t\right)} \tag{38}$$

The peripheral velocity U, m/s is calculated based on jet velocity:

$$U = \mathrm{SR} \times V_j \tag{39}$$

The turbine wheel diameter D_w, m:

$$D_w = \frac{60 \times U}{\pi \times \mathrm{RPM}} \tag{40}$$

The jet diameter d_j, m is calculated based on wheel diameter and diameter ratio DR:

$$d_j = D_w \times \mathrm{DR} \tag{41}$$

The discharge Q_{PWT}, m³/s is calculated based on turbine shaft power $\mathrm{SHP}_{\mathrm{PWT}}$, total efficiency, and total head H_t:

$$Q_{\mathrm{PWT}} = \frac{1{,}000 \times \mathrm{SHP}_{\mathrm{PWT}}}{\eta_{\mathrm{total}} \times \rho \times g \times H_t} \tag{42}$$

Number of jets n_j based on discharge, jet velocity, and jet diameter:

$$n_j = \frac{4 \times Q}{V_j \times \pi \times d_j^2} \tag{43}$$

Turbine specific speed V_{PWT}, rad/s:

$$V_{\mathrm{PWT}} = \frac{2 \times \pi \times \mathrm{RPM}}{60} \times \frac{\sqrt{\left(1000 \times \mathrm{SHP}_{\mathrm{PWT}}\right)/\rho}}{\left(g \times H_t\right)^{5/4}} \tag{44}$$

C.2. Centrifugal pump model [31,31,46]:

The centrifugal pump discharge, m³/s is calculated based on the hydro storage tank and operating hours:

$$Q_{\mathrm{cent}} = \frac{\mathrm{Vol}}{\mathrm{OH} \times 3600} \tag{45}$$

The centrifugal pump head losses, m is calculated based on pump discharge Q_{cent}, tubes cross section area A_t, flow velocity V_f, Reynold's number and loss coefficient f:

$$V_f = f\left(Q_{\mathrm{cent}}, A_t\right), R_e = \frac{\rho V_f D_t}{\mu}, f = f\left(\mathrm{Re}\right) \tag{46}$$

Total tube length through the system based on static head H_s, and tank head, H_{tnk}, m:

$$L_t = H_s + H_{\mathrm{tnk}} \tag{47}$$

The head loss H_{loss} is then calculated based on total tube length L_t, major and minor losses:

$$H_{\mathrm{loss}} = \frac{f \times L_t}{2gD_t} + \frac{K}{2g} \tag{48}$$

and the total pumping head H_{cent}, m, is:

$$H_{\mathrm{cent}} = \left(\frac{Q_{\mathrm{cent}}}{A_t}\right)^2 \times H_{\mathrm{loss}} + H_s + H_{\mathrm{tnk}} \tag{49}$$

and the centrifugal pump power, kW:

$$\mathrm{SHP}_{\mathrm{cent}} = \frac{\rho g \times Q_{\mathrm{cent}} \times H_{\mathrm{cent}}}{1000 \times \eta_{\mathrm{cent}}} \tag{50}$$

Appendix-D: Cost analysis

RO membrane cost, MC (~60% of direct capital costs DCC) $, [8,9]:

$$\mathrm{MC} = 0.6 \times \mathrm{DCC} \tag{51}$$

Membrane annual replacement cost, ARC (~10% of membrane purchase cost, MC) $, [8,9]:

$$\mathrm{ARC} = 0.1 \times \mathrm{MC} \tag{52}$$

where, the direct capital costs is DCC = M_d × 1,000, $

The amortization factor a_f based on plant life time parameter, LTP, 1/y, and interest rate, ir is then calculated:

$$a_f = \mathrm{ir} \times \frac{\left(1+\mathrm{ir}\right)^{\mathrm{LTP}}}{\left(1+\mathrm{ir}\right)^{\mathrm{LTP}} - 1} \tag{53}$$

RO calculate the annual fixed charges, AFC $/y [8,9,30,31]:

$$\mathrm{AFC} = a_f \times \mathrm{DCC} \tag{54}$$

RO calculate the annual chemicals cost, ACHC $/y [8,9,30,31] based on specific chemical costs = 0.033$/m³, load factor = 0.9, and productivity, M_d, m³/d:

$$\mathrm{ACHC} = 0.033 \times 0.9 \times M_d \times 365 \tag{55}$$

RO Calculate the annual labor cost, ALC $/y, based on specific labor cost = 0.05$/m³, and productivity, M_d, m³/d:

$$\mathrm{ALC} = 0.05 \times 0.9 \times M_d \times 365 \tag{56}$$

Annual CSGE costs $/y [34–38]:

$$\mathrm{ACSGETC} = \mathrm{CSGEC}t \times a_f \tag{57}$$

where,

$$\mathrm{CSGEC}t = \mathrm{DCC} = f\left(\begin{matrix}\mathrm{Dc} \times A_{\mathrm{dish}} + \mathrm{Rc} \times P_{\mathrm{total}} + \mathrm{Engc} \times P_{\mathrm{total}} + \\ \mathrm{Sitec} \times A_{\mathrm{total}}\end{matrix}\right) + \left(0.15 \times \mathrm{DCC} + \mathrm{OM}c \times P_{\mathrm{total}}\right) \tag{58}$$

$$\mathrm{Dc\ Dish\ costs} = \frac{300\$}{\mathrm{m}^2}, \mathrm{Rc\ receiver\ costs} = \frac{185\$}{\mathrm{kW}},$$

$$\mathrm{Engc\ Engine\ costs} = \frac{400\$}{\mathrm{kW}}, \mathrm{Sitec\ site\ costs} = \frac{2.2\$}{\mathrm{m}^2},$$

$$\mathrm{OM\ operational\ costs} = \frac{37\$}{\mathrm{kW\ y}}$$

Annual hydropower costs $/y [30,31,46]:

$$\text{AHydroC} = \text{HydroC}t \times a_f \tag{59}$$

where,

$$\text{HydroC}t = \left(1{,}000 \sim 8{,}000, \frac{\$}{\text{kW}}\right) \times \text{SHP}_{\text{PWT}} \tag{60}$$

Calculate total annual cost, ATC, $/y:

$$\text{ATC} = \text{ARC} + \text{AFC} + \text{ACHC} + \text{ALC} + \text{ACSGETC} + \text{AHydroC} \tag{61}$$

Calculate the total water price, TWP, $/m^3:

$$\text{TWP} = \frac{\text{ATC}}{0.9 \times M_d \times 365} \tag{62}$$